

# A New Particle Filter for Target Tracking in MIMO OFDM Integrated Sensing and Communications

Shixiong Wang, Wei Dai, and Geoffrey Ye Li, *Fellow, IEEE*

arXiv:2512.09098v1 [eess.SP] 9 Dec 2025

**Abstract**—Particle filtering for target tracking using multi-input multi-output (MIMO) pulse-Doppler radars faces three long-standing obstacles: a) the absence of reliable likelihood models for raw radar data; b) the computational and statistical complications that arise when nuisance parameters (e.g., complex path gains) are augmented into state vectors; and c) the prohibitive computational burden of extracting noisy measurements of range, Doppler, and angles from snapshots. Motivated by an optimization-centric interpretation of Bayes’ rule, this article addresses these challenges by proposing a new particle filtering framework that evaluates each hypothesized state using a tailored cost function, rather than relying on an explicit likelihood relation. The framework yields substantial reductions in both running time and tracking error compared to existing schemes. In addition, we examine the implementation of the proposed particle filter in MIMO orthogonal frequency-division multiplexing (OFDM) systems, aiming to equip modern communication infrastructure with integrated sensing and communications (ISAC) capabilities. Experiments suggest that MIMO-OFDM with pulse-Doppler processing holds considerable promise for ISAC, particularly when wide bandwidth, extended on-target time, and large antenna aperture are utilized.

**Index Terms**—Particle Filter, Gibbs Posterior, Target Tracking, MIMO, OFDM, ISAC, Pulsed Radar, Continuous-Wave Radar, Coordinated Multi-Point, Ambiguity Function, Entropy Method.

## I. INTRODUCTION

In emerging wireless systems, integrated sensing and communications (ISAC) has been envisioned as a promising solution for enabling both communication and sensing functions on a common hardware platform, leveraging shared resources in power, time, space, and frequency, such as transmit and receive antennas, radio frequency chains, digital signal processing units, and transmit waveforms [1], [2]. This integration can reduce hardware volume, improve resource efficiency, and provide mutual benefits between sensing and communications [3], [4]. Among many sensing aspects (e.g., detection, measuring, tracking, and imaging [5]), target tracking is fundamental and plays a critical role in a broad range of ISAC applications, such as sensing-assisted communications [3] and intelligent transportation [6]. This article is concerned with target tracking problems in ISAC. Particularly, the multi-input multi-output orthogonal frequency-division multiplexing (MIMO-OFDM) systems are investigated for three reasons. First, MIMO technology enables spatial and waveform diversity to enhance communication performance in terms of throughput and reliability [7]–[9], as well as radar sensing performance in

terms of angle resolution and spatial interference suppression [10]–[12]. Second, OFDM techniques allow frequency-domain signal processing using fast Fourier transform (FFT) if the duration of the cyclic prefix is sufficient to cover all round-trip target delays [13, p. 19], [14], which brings significant computational benefits to real-world radar operations [15], [16], [17, Eqs. (62)–(63)], especially compared to time-domain integration-based matched filtering for ranging [18], [19]. Third, modern mature wireless communication systems are built upon MIMO-OFDM, such as 4G LTE, 5G NR, Wi-Fi 5/6/6E/7, and even upcoming 6G schemes; the adoption of MIMO-OFDM in 6G has been confirmed by the 3GPP RAN1 Committee in August 2025. Therefore, it is natural to equip these widespread systems with sensing capabilities without requiring large-scale infrastructure modification and software upgradation [13], [15]. Research on MIMO ISAC, OFDM ISAC, and MIMO-OFDM ISAC is flourishing. Remarkable progress in this and related areas includes the following: 1) information-theoretic analyses of systematic and methodological performances [20]–[23]; 2) signal processing methods in target detection and parameter estimation [16], [24]–[26], waveform design [14], [27], [28], beamforming and precoding [29], [30], and pulse shaping and modulation [31], [32]; 3) and practical developments of real-world systems [33]. Target tracking for MIMO-OFDM ISAC systems is also reported, although sparsely, such as [34], where only angles are tracked.

The target tracking problem for a single object can be formulated as [35], [36]

$$\begin{cases} \mathbf{x}_k = \mathbf{f}_k(\mathbf{x}_{k-1}, \mathbf{w}_{k-1}) \\ \mathbf{y}_k = \mathbf{h}_k(\mathbf{x}_k, \mathbf{v}_k), \end{cases} \quad (1)$$

where  $k = 0, 1, 2, \dots$  denotes the discrete time index,  $\mathbf{x}_k \in \mathbb{R}^{d_x}$  the target state vector,  $\mathbf{y}_k \in \mathbb{R}^{d_y}$  (or  $\mathbf{y}_k \in \mathbb{C}^{d_y}$ ) the measurement vector,  $\mathbf{f}_k(\cdot, \cdot)$  the state transition function,  $\mathbf{w}_k \in \mathbb{R}^{d_w}$  the process noise vector,  $\mathbf{h}_k(\cdot, \cdot)$  the state measurement function, and  $\mathbf{v}_k \in \mathbb{R}^{d_v}$  (or  $\mathbf{v}_k \in \mathbb{C}^{d_v}$ ) the measurement noise vector. Mathematically, a target tracking problem is stated as using the system model (1) and the measurement history  $\mathcal{Y}_k := \{\mathbf{y}_0, \mathbf{y}_1, \dots, \mathbf{y}_k\}$ , up to and including time  $k$ , to infer the unknown states  $\mathbf{x}_k$  of the target, using nonlinear state estimation approaches, such as particle filtering [37], [38, Chap. 15], [39], which constitutes the technical focus of this article. The state vector  $\mathbf{x}_k$ , as per specific applications, can consist of different variables. On the one hand, in Cartesian coordinates,  $\mathbf{x}_k$  can denote positions, velocities, and accelerations of the target of interest (ToI) in two- or three-dimensional spaces [35]. On the other hand, in polar coordinates,  $\mathbf{x}_k$  can include range, radial speed (or Doppler frequency shift), angles

S. Wang, W. Dai, and G. Y. Li are with the Department of Electrical and Electronic Engineering, Imperial College London, London SW7 2AZ, United Kingdom (E-mails: s.wang@u.nus.edu; wei.dai1@imperial.ac.uk; geoffrey.li@imperial.ac.uk). (Corresponding Author: S. Wang.)

(e.g., elevation, azimuth), and angular speeds of the ToI in the radar's view field [40], [41]. At times, statistical signal processing methods mandate  $\mathbf{x}_k$  to contain some nuisance parameters, for example, the turning rate in a coordinated-turn maneuvering model [35], the model index in a multi-model tracking system [42], or the real and imaginary components of complex path gains [34], [36], [40], [41]. According to the level of radar signal processing, the following two cases for the measurement vector  $\mathbf{y}_k$  are standard:

- *Information-Level Tracking*: In this scheme,  $\mathbf{y}_k \in \mathbb{R}^{d_y}$  denotes the radar's measurements of range, radial velocity, and angle(s) that are to be assimilated by the target's motion mechanism (1); see, e.g., [5, Chap. 7]. At times,  $\mathbf{y}_k \in \mathbb{R}^{d_y}$  can also denote the unfiltered positions and velocities of the ToI, calculated using raw range-Doppler-angle measurements [43], [44, p. 8]. This is the most common way in real-world radar target tracking due to its simplicity in operation. When detection is jointly considered, this paradigm is widely referred to as *detect-then-track* in the literature [45].
- *Signal-Level Tracking*: In this scheme,  $\mathbf{y}_k \in \mathbb{C}^{d_y}$  denotes the radar's base-band raw in-phase/quadrature (I/Q) snapshots [36], [40], [41], [46]. Note that, within a target tracking period  $k$ , a radar can collect several snapshots in fast and slow times; see [5, Sec. 1.5.1]. When detection is jointly considered, this paradigm is known as *track-before-detect*, which outperforms detect-then-track in the low signal-to-noise ratio (SNR) regimes [47], [48].

However, three drawbacks of the existing schemes for radar target tracking have to be outlined:

- In information-level tracking, at each time  $k$ , obtaining measurements  $\mathbf{y}_k$  and calibrating their uncertainty quantification parameters (i.e., distribution type, mean, covariance, and other statistics of  $\mathbf{v}_k$ ) are computationally prohibitive, especially when advanced optimization techniques, such as compressed sensing and tensor decomposition, are utilized; see [25], [26], [49, Table II]. Even for matched-filter-based methods that are considered computationally efficient [16], searching for the peaks of the filter outputs in a validation gate is time-consuming as well. The computational burden further increases when particle filtering is afterward employed to link these measurements  $\mathbf{y}_k$  with the tracking model (1).
- In signal-level tracking, when raw snapshots  $\mathbf{y}_k$  are obtained, the next key step is to calculate the likelihoods  $q(\mathbf{y}_k|\mathbf{x}_k)$  of hypothesized states  $\mathbf{x}_k$ ; note that the likelihood function  $q(\mathbf{y}_k|\mathbf{x}_k)$  is induced by the measurement model  $\mathbf{y}_k = \mathbf{h}_k(\mathbf{x}_k, \mathbf{v}_k)$  in (1). The challenge is that the measurement model  $\mathbf{y}_k = \mathbf{h}_k(\mathbf{x}_k, \mathbf{v}_k)$  is unknown (or uncertain) in practice, so is the probabilistic model  $q(\mathbf{y}_k|\mathbf{x}_k)$ , because the information about environmental scatterers (including targets of no interest) and channel noises is lacking. Assuming inexact distribution families or statistics for  $q(\mathbf{y}_k|\mathbf{x}_k)$  cannot offer trustworthy likelihood information.
- To handle unknown parameters involved in the state transition and measurement mechanisms, we usually need

to include the nuisance parameters into the state vector  $\mathbf{x}_k$ , e.g., the turning rate of the coordinated turn model [35], the real and imaginary components of the complex path gain due to the ToI [40], [41]. However, this operation imposes nontrivial complications because the statistical and computational efficiency of particle filters significantly deteriorate when the dimension  $d_x$  of the state vector  $\mathbf{x}_k$  increases [50], [51]. Even though the Rao-Blackwellized (i.e., marginalized) particle filtering [52], [53] has the potential to mitigate such complications, it remains inadequate for tracking rapidly jumping nuisance parameters if an accurate state-transition model for these parameters is not available. For example, complex path gains can change abruptly across consecutive tracking periods  $k$  for fast-fading channels, so the usual first-order Gauss-Markov models (e.g., random walk and constant-velocity models) are not appropriate; see the experiment section for a specific discussion.

To address the above issues of radar target tracking, this article proposes a new particle filtering framework for signal-level target tracking (PF-SLTR), by leveraging the optimization-centric interpretation of Bayes' rule, i.e., the Gibbs posterior [54]–[56]. The advantages of this new framework are threefold:

- We do not require an operationally separate, and computationally expensive, phase to obtain raw radar measurements (e.g., range, Doppler, angles) and calibrate their uncertainty quantification.
- We do not mandate the knowledge of the probabilistic model  $q(\mathbf{y}_k|\mathbf{x}_k)$  to calculate  $\mathbf{y}_k$ -data evidence (i.e., likelihoods) of particles (i.e., hypothesized state values).
- We do not augment the parameters of the complex path gain, due to the ToI, into the state vector.

Technically, the pivotal yet challenging step is to devise an efficient cost function  $h(\mathbf{y}_k, \mathbf{x}_k)$  to quantify the  $\mathbf{y}_k$ -data evidence of a hypothesized state  $\mathbf{x}_k$ , which requires problem-specific investigation for signal-level target tracking using MIMO radar. Existing general principles and methodologies in applied statistics and machine learning are not directly applicable because the design of  $h$  is domain-specific and there is no one-size-fits-all solution; cf., e.g., [54]–[58].

Moreover, we adapt the proposed PF-SLTR to MIMO-OFDM ISAC systems, where MIMO-OFDM communication waveforms are reused for high-accuracy target tracking. Radar signal processing for target tracking in both the time domain and the frequency domain is investigated, corresponding to the pulsed radar scheme [59] and the continuous-wave radar scheme [13], [14], respectively. Two highlights are as follows:

- The pulsed scheme is appropriate for far and fast targets, and the maximum identifiable range is determined by the duration of the pulse repetition interval. In this case, MIMO-OFDM communication signals are treated as ordinary radar waveforms, and usual pulse-Doppler processing is applied; see, e.g., [5, Chaps. 4-5]. In contrast, the continuous-wave (CW) scheme is tailored for near and slow targets, and the maximum identifiable range is limited by the duration of the cyclic prefix (CP) [1], [13]. Therefore, the pulsed case is *sensing*-

*centric*, where the use of radar silent times (i.e., small duty cycle) compromises the communication throughput but increases the ranging capacity, while the CW case is *communications-centric*, where the duration of CP limits the ranging capacity but the usual MIMO-OFDM communications can remain unaffected.

- In the pulsed paradigm, the circular convolution property of the FFT processing cannot be guaranteed. Hence, matched filtering for ranging must be carried out in the time domain using time-correlation methods [18], although algorithmically, the computational complexity of time correlation can be reduced by zero-padding and FFT tricks; see [5, p. 678]. Contrarily, in the CW paradigm, the circular convolution property of the FFT processing is ensured because the CP duration can cover all path delays. As a result, matched filtering for ranging can be directly performed in the frequency domain using FFT [15], [16], [17, Eqs. (62)-(63)]. Note that matched filtering in the CW case requires the removal of CPs [14], while that in the pulsed case mandates the preservation of CPs [59].

For clarity of presentation in developing the new particle filter, and without loss of generality, this article focuses exclusively on pure target tracking and does not consider the detection problem. The extension to joint detection and tracking is technically straightforward; one can just replace the canonical particle filters with the proposed PF-SLTR. Additionally, the multi-target joint-tracking problem is deferred to future work, as it demands a substantially larger research effort. For extensive and comparative readings on these two directions, see, e.g., [47], [48], [60]–[62].

*Primary Contributions:* In summary, the contributions of this article can be outlined as follows: 1) A new particle filtering framework for signal-level target tracking is studied, which frees practitioners from obtaining raw range-Doppler-angle measurements, specifying the exact likelihood model, and augmenting path gain parameters into the state vector; 2) The usage of the proposed PF-SLTR in MIMO-OFDM ISAC systems is investigated, by designing waveform structures and signal processing chains.

*Supplementary Contribution:* To extend the applicability of PF-SLTR to coordinated multi-point systems and achieve performance gains from cross-station synergy, we further develop a fusion strategy for particle-represented posterior distributions that are generated by different ISAC stations; see Appendix A for better readability, as well as due to the page limit.

*Notations:* Let  $\mathbb{R}^d$  and  $\mathbb{C}^d$  denote the  $d$ -dimensional spaces of real and complex numbers, respectively. We use lowercase letters for vectors (e.g.,  $\mathbf{x}$ ) and uppercase ones for matrices (e.g.,  $\mathbf{X}$ ), both in boldface; scalars are not boldfaced. Random quantities are written in Roman fonts (e.g.,  $\mathbf{x}$ ,  $\mathbf{X}$ ), while deterministic ones are in italic fonts (e.g.,  $\mathbf{x}$ ,  $\mathbf{X}$ ). Let  $\langle x \rangle$  denote the rounding operation of real number  $x$  to the nearest integer, and  $[N] := \{0, 1, 2, \dots, N-1\}$  the running index set starting from zero for integer  $N$ . Let  $\mathbf{I}_d$  denote the  $d$ -dimensional identity matrix, and  $\mathbf{X}^T$  and  $\mathbf{X}^H$  the transpose and conjugate transpose of matrix  $\mathbf{X}$ , respectively.

## II. SYSTEM MODEL AND PROBLEM STATEMENTS

### A. System Model of Signal-Level Target Tracking

Since this article focuses on the reuse of wireless communication signals for sensing, in this section, we review the MIMO multi-carrier pulse-Doppler radar model that is suitable for various transmit waveforms. For conciseness of presentation and without loss of generality, this article specifically investigates a two-dimensional planar target tracking problem so that only one direction-of-arrival (DoA) angle for each target is to be examined. We consider a mono-static ISAC station that is

- Located at the origin  $[0, 0]$  and staying unmoving.
- Operating with center frequency  $f_c$ , wavelength  $\lambda$ , bandwidth  $B$ , sampling time period  $T_s = 1/B$ , per-antenna transmit power budget  $P_t$ .
- Equipped with a transmit antenna array that includes  $N_t$  collocated omnidirectional elements; the transmit steering vector is  $\mathbf{a}(\theta)$  in direction  $\theta$ , which is determined by the array geometry.
- Equipped with a receive antenna array that includes  $N_r$  collocated omnidirectional elements; the receive steering vector is  $\mathbf{b}(\theta)$  in direction  $\theta$ . The receive array and transmit array can operate in either the time-division duplex mode (cf. pulsed radars) or the full-duplex mode (cf. continuous-wave radars that employ pulse-Doppler processing).
- Configured with target tracking period  $T_t$ , i.e., the time interval between  $k-1$  and  $k$  in (1).

For waveform structures in terms of sensing, we assume that

- Each target tracking period  $T_t$  includes one coherent processing interval (CPI)  $T_i$ , within which the motion parameters of the ToI remain unchanged and can be resolved. Note that  $T_i \leq T_t$ .
- Each CPI constitutes  $N_p$  pulses (i.e.,  $N_p$  slow times) and each pulse has a time duration  $T_p$ . Hence, the number of snapshots within a pulse is  $L_{ss} = \langle T_p/T_s \rangle$ .
- The pulse repetition interval (PRI) is  $T_r$ , and therefore, the pulse repetition frequency (PRF) is  $f_r = 1/T_r$ . Note that  $T_p \leq T_r \leq T_i \leq T_t$ .
- Each PRI consists of  $L$  sampling points, so  $T_r = LT_s$ . The set  $[L]$  defines  $L$  range bins; note that  $L_{ss} \leq L$ .

The above pulse-Doppler radar configurations imply that

- We have the CPI  $T_i = N_p T_r$ .
- The resolutions of round-trip delay and Doppler frequency are  $1/B$  and  $1/T_i$ , respectively.
- The inter-pulse silent time is  $T_r - T_p$ .
- The maximum detectable round-trip delay is  $\tau_{\max-d} = T_r - T_p$ , and therefore, the maximum radar detection distance is  $R_{\max-d} = C\tau_{\max-d}/2$ ;  $C$  is the light speed. The minimum detectable round-trip delay is  $\tau_{\min-d} = T_p$  if the time-division duplex mode is adopted, or  $\tau_{\min-d} = 0$  if the full-duplex mode is employed;  $R_{\min-d} := C\tau_{\min-d}/2$ .
- The minimum and maximum unambiguous Doppler frequency shifts are  $\nu_{\min-ua} = -f_r/2$  and  $\nu_{\max-ua} = f_r/2$ , respectively.

In addition, suppose that the ToI within the tracking time period  $k$  is characterized by

- The true round-trip delay  $\tau_0$ , and hence, the true range  $R_0 = C\tau_0/2$ . (Note that  $R_{\min\text{-d}} \leq R_0 \leq R_{\max\text{-d}}$ .)
- The true Doppler frequency shift  $\nu_0$ , and therefore, the true radial speed  $v_0 = \nu_0\lambda/2$ . (Note that  $\nu_{\min\text{-ua}} \leq \nu_0 \leq \nu_{\max\text{-ua}}$ .)
- The true DoA  $\theta_0$  relative to the array boresight. (The transmit array and receive array are supposed to have the same DoA  $\theta_0$  for the ToI.)

With the above system settings, in a given target tracking period  $k$ , the sensing mechanism of narrowband MIMO radars<sup>1</sup> can be modeled as [19, Eq. (11)], [63, p. 439], [49],

$$\mathbf{y}(t) = \beta_0 \mathbf{b}(\theta_0) \mathbf{a}^H(\theta_0) \mathbf{s}(t - \tau_0) e^{j2\pi\nu_0 t} + \sum_{i=1}^{N_s} \beta_{i,0} \mathbf{b}(\theta_{i,0}) \mathbf{a}^H(\theta_{i,0}) \mathbf{s}(t - \tau_{i,0}) e^{j2\pi\nu_{i,0} t} + \mathbf{n}(t), \quad (2)$$

where  $t$ ,  $0 \leq t \leq T_i \leq T$ , denotes the radar's logical time of signal processing in a CPI;  $\beta_0$  is the path gain of the ToI;  $N_s$  is the total number of scatterers (including, e.g., targets of no interest);  $\beta_{i,0}$ ,  $\theta_{i,0}$ ,  $\tau_{i,0}$ , and  $\nu_{i,0}$  are the parameters of the  $i^{\text{th}}$  scatterer;  $\mathbf{s}(t) \in \mathbb{C}^{N_t}$  denotes the transmitted waveform at time  $t$ ,  $\mathbf{y}(t) \in \mathbb{C}^{N_r}$  the received signal, and  $\mathbf{n}(t) \in \mathbb{C}^{N_r}$  the zero-mean circularly-symmetric complex Gaussian channel noise vector. For a target tracking problem aiming to resolve target parameters  $(\tau_0, \nu_0, \theta_0)$ , (2) can be compactly written as

$$\mathbf{y}(t) = \beta_0 \mathbf{b}(\theta_0) \mathbf{a}^H(\theta_0) \mathbf{s}(t - \tau_0) e^{j2\pi\nu_0 t} + \mathbf{n}_c(t), \quad (3)$$

where  $\mathbf{n}_c(t) \in \mathbb{C}^{N_r}$  denotes the channel interference-plus-noise (IPN) vector, which is not necessarily Gaussian. Supposing that the Doppler frequency shift is piece-wise constant across different PRIs, (3) can be sampled at  $t = pT_r + lT_s$ , leading to the discrete-time representation

$$\mathbf{y}_p(l) = \beta_0 \mathbf{b}(\theta_0) \mathbf{a}^H(\theta_0) \mathbf{s}_p(l - \tau_0) e^{j2\pi\nu_0 pT_r} + \mathbf{n}_{c,p}(l), \quad (4)$$

where  $p \in [N_p]$  is the slow-time Doppler-bin index and  $l \in [L]$  is the fast-time range-bin index;  $\mathbf{s}_p(l)$  is the sampled transmitted waveform at  $p^{\text{th}}$  PRI and  $l^{\text{th}}$  range bin,  $\mathbf{y}_p(l)$  the sampled received signal, and  $\mathbf{n}_{c,p}(l)$  the sampled channel IPN vector. To avoid notational clutter,  $\mathbf{s}_p(l - \tau_0)$  is shorthand for  $\mathbf{s}_p(l - \langle \tau_0/T_s \rangle)$ .

At times, the frequency-domain representation of (4) would be computationally useful. Suppose that we have  $N_{\text{cr}}$  FFT points for ranging. Let the frequency-bin width be  $\Delta := B/N_{\text{cr}}$ . Then, the frequency-domain representation of (4) is

$$\bar{\mathbf{y}}_p(n) = \beta_0 \mathbf{b}(\theta_0) \mathbf{a}^H(\theta_0) \bar{\mathbf{s}}_p(n) e^{-j2\pi n \Delta \tau_0} e^{j2\pi p T_r \nu_0} + \bar{\mathbf{n}}_{c,p}(n), \quad (5)$$

where  $n \in [N_{\text{cr}}]$  denotes the frequency-bin index,  $\bar{\mathbf{y}}_p$  the FFT of  $\mathbf{y}_p$ ,  $\bar{\mathbf{s}}_p$  the FFT of  $\mathbf{s}_p$ , and  $\bar{\mathbf{n}}_{c,p}$  the FFT of  $\mathbf{n}_{c,p}$ ; the center-frequency-dependent phase term  $e^{-j2\pi f_c \tau_0}$  has been absorbed by  $\beta_0$ . In matched filtering for ranging, it is common that  $N_{\text{cr}} = L$ . However, the computational complexity in the time domain is  $\mathcal{O}(L^2)$ , while that in the frequency domain is  $\mathcal{O}(L \log_2(L))$  due to the FFT technique.

<sup>1</sup>When a wireless system is narrowband in terms of radar sensing, it may still be treated as broadband in terms of communications; for determination criteria, see [19, Eq. (3)], [63, p. 439].

In signal-level target tracking (SLTR), (4) or (5) defines the state measurement equation in the tracking model (1). To be specific,  $\mathbf{y}_k$  is a data set constructed as

$$\mathbf{y}_k := \begin{cases} \{\mathbf{y}_p(l)\}_{\forall p,l}, & \text{if time-domain processing,} \\ \{\bar{\mathbf{y}}_p(n)\}_{\forall p,n}, & \text{if frequency-domain processing,} \end{cases} \quad (6)$$

where the notational dependence of the right-hand-side terms on the tracking period index  $k$  is omitted.

Under the Bayesian statistical inference paradigm, the target tracking problem using the system model (1), in a specific time  $k$ , can be stated as finding the posterior distribution

$$q(\mathbf{x}_k | \mathcal{Y}_k) \propto q(\mathbf{y}_k | \mathbf{x}_k) q(\mathbf{x}_k | \mathcal{Y}_{k-1}) \quad (7)$$

of the unknown state vector  $\mathbf{x}_k$  by utilizing the likelihood function  $\mathbf{x}_k \mapsto q(\mathbf{y}_k | \mathbf{x}_k)$  and the prior distribution  $q(\mathbf{x}_k | \mathcal{Y}_{k-1})$ ; at every  $k$ , the unknown true state vector  $\mathbf{x}_{0,k}$  is one-to-one corresponded to the true target parameters  $(\tau_{0,k}, \nu_{0,k}, \theta_{0,k})$ . It is preferable if  $q(\mathbf{x}_k | \mathcal{Y}_k)$  can concentrate around the true state  $\mathbf{x}_{0,k}$ . The prior distribution  $q(\mathbf{x}_k | \mathcal{Y}_{k-1})$  is induced by the state transition equation, while the likelihood function  $q(\mathbf{y}_k | \mathbf{x}_k)$  is defined by the state measurement equation. In this section, for notational simplicity, we suppress the dependence on the time index  $k$  and the measurement history  $\mathcal{Y}_{k-1}$ . Eq. (7) is therefore shorthanded as

$$q(\mathbf{x} | \mathbf{y}) \propto q(\mathbf{y} | \mathbf{x}) q(\mathbf{x}). \quad (8)$$

Focusing on the target parameters, (8) particularizes into

$$q(\boldsymbol{\varphi} | \mathbf{y}) \propto q(\mathbf{y} | \boldsymbol{\varphi}) q(\boldsymbol{\varphi}), \quad (9)$$

where  $\boldsymbol{\varphi} := (\tau, \nu, \theta) \in \mathbb{R}^3$  and the likelihood function  $\boldsymbol{\varphi} \mapsto q(\mathbf{y} | \boldsymbol{\varphi})$  is induced by either (4) or (5); cf. (6).

## B. Problem Statements (Research Gaps in SLTR)

In applying the Bayes' rule (9) to signal-level target tracking, the real-world operational dilemma is twofold:

- The explicit and exact mathematical expression of the likelihood function  $\boldsymbol{\varphi} \mapsto q(\mathbf{y} | \boldsymbol{\varphi})$  is difficult to obtain because the probabilistic models of  $\beta_0$ ,  $\mathbf{n}_{c,p}(l)$ , and  $\bar{\mathbf{n}}_{c,p}(n)$  are challenging to specify in practice. Even if the probabilistic form of  $q(\mathbf{y} | \boldsymbol{\varphi})$  is (assumed to be) known, for example, Gaussian or exponential family, its statistical information, such as mean and covariance, is still to be meticulously calibrated by leveraging the domain knowledge and historical data. The complication arises if  $q(\mathbf{y} | \boldsymbol{\varphi})$  is time-varying across different tracking periods due to the significant maneuvers of the ToI and scatterers and to the change of channel conditions.
- To simplify the modeling of  $q(\mathbf{y} | \boldsymbol{\varphi})$ , some statistical inference methods, such as conventional particle filters, treat  $\beta_0$  as a nuisance parameter to be jointly estimated from the collected data [40], [41]. This scheme leads to the augmented parameter vector  $\boldsymbol{\varphi} := (\text{real}(\beta), \text{imag}(\beta), \tau, \nu, \theta) \in \mathbb{R}^5$  of the ToI. However, although convenient for modeling, this augmentation significantly introduces additional computational burdens to statistical inference because the larger the dimension

of the state vector  $\mathbf{x}_k$  is, the lower the computational and sample efficiency of any statistical inference method would be. This is specifically the case for particle filters where more particles, and therefore more computational resources, must be employed to guarantee a satisfactory accuracy for  $(\tau_0, \nu_0, \theta_0) \in \mathbb{R}^3$  [50], [51]. Although the Rao-Blackwellized particle filtering can be used to reduce such computational burdens [52], it is inadequate if  $\beta_0$  abruptly varies across consecutive tracking periods  $k$ : Note that to track an unknown parameter, it should remain almost constant or slowly vary over time  $k$  [38, p. 397].

To address the above two issues, this article revolutionizes the existing particle filtering framework for signal-level target tracking and proposes a new PF-SLTR scheme.

### III. A NEW PARTICLE FILTER FOR SIGNAL-LEVEL TARGET TRACKING USING MIMO RADAR

#### A. Optimization-Centric Interpretation of Bayes' Rule (9)

In the statistical machine learning and general statistics communities, a well-established optimization-centric interpretation of the Bayes' Rule (9) is as follows:

$$q(\varphi|\mathbf{y}) = \underset{u(\varphi)}{\operatorname{argmin}} \mathbb{E}_{\varphi \sim u(\varphi)} [-\ln q(\mathbf{y}|\varphi)] + \text{KL}[u(\varphi) \| q(\varphi)], \quad (10)$$

where  $u(\varphi)$  is a variable distribution of  $\varphi$  and  $\text{KL}[u(\varphi) \| q(\varphi)]$  defines the Kullback–Leibler divergence of  $u(\varphi)$  from  $q(\varphi)$ . Eq. (10) indicates that the posterior distribution  $q(\varphi|\mathbf{y})$  of  $\varphi$ , given  $\mathbf{y}$ , maximizes the expected log-likelihood evaluated at  $\mathbf{y}$ , and simultaneously, minimizes the dissimilarity from the prior distribution  $q(\varphi)$ . This interpretation aligns well with our intuition: the posterior distribution should mostly match the “data evidence” at hand (i.e., maximum likelihood), and at the same time, mostly match the “prior knowledge” in the brain (i.e., minimum deviation from the prior).

Eq. (10) can be generalized to the following formulation

$$q(\varphi|\mathbf{y}) = \underset{u(\varphi)}{\operatorname{argmin}} \mathbb{E}_{\varphi \sim u(\varphi)} \xi h(\mathbf{y}, \varphi) + \text{KL}[u(\varphi) \| q(\varphi)], \quad (11)$$

where  $h(\mathbf{y}, \varphi)$  is a general cost function that encodes the  $\mathbf{y}$ -data evidence of  $\varphi$ , beyond the well-adopted negative log-likelihood cost function  $-\ln q(\mathbf{y}|\varphi)$ , and  $\xi \geq 0$  is a tradeoff parameter that balances between  $\mathbf{y}$ -data evidence and  $q(\varphi)$ -prior information. The generalization from (10) to (11) is rooted in the following two motivations:

- Different applications prefer different utility metrics, so we can manipulate how the available data  $\mathbf{y}$  supports the utility of the solution (or decision)  $\varphi$ . The basic principle to design  $h$  is that, if  $\varphi_1$  is favored over  $\varphi_2$  given  $\mathbf{y}$ , we should have  $h(\mathbf{y}, \varphi_1) \leq h(\mathbf{y}, \varphi_2)$ . Illustrating instances in machine learning applications can be seen in [54].
- In practice, the likelihood function  $q(\mathbf{y}|\varphi)$  may not be exactly specified, so we can steer the cost function  $h$  to achieve robustness against this likelihood-model mismatch. Examples in this direction can be seen in [56].

A desired property of (11) is that it admits a closed-form solution for every cost function  $h(\mathbf{y}, \varphi)$  and every prior distribution  $q(\varphi)$ , which is beneficial in real-time signal processing, such as online target tracking.

*Lemma 1* (see [55]): The generalized posterior distribution  $q(\varphi|\mathbf{y})$  solving (11) is given by

$$q(\varphi|\mathbf{y}) \propto q(\varphi) e^{-\xi h(\mathbf{y}, \varphi)}, \quad (12)$$

if the normalizer of the right-hand-side term exists.  $\square$

Eq. (12) is called the *Gibbs posterior* in the literature. Focusing back on the Bayesian filtering for signal-level target tracking (e.g., PF-SLTR), since the exact likelihood function  $\varphi \mapsto q(\mathbf{y}|\varphi)$  is unavailable, we are motivated to construct an appropriate cost function  $h(\mathbf{y}, \varphi)$  to solve the two issues stated before, that is, without relying on the exact knowledge of the likelihood function  $\varphi \mapsto q(\mathbf{y}|\varphi)$  and without augmenting nuisance parameters ( $\text{real}(\beta)$ ,  $\text{imag}(\beta)$ ) into  $\varphi$ .

#### B. A New Framework of PF-SLTR

Particle filtering, which utilizes particle representations of probability density functions, is a computational method of Bayesian filtering [37], [39]. To be specific, in particle filtering, the prior distribution  $q(\varphi)$  is represented by a set of discrete particles  $\{\varphi_0, \varphi_1, \dots, \varphi_{N_{\text{par}}-1}\}$ :

$$q(\varphi) = \sum_{i=0}^{N_{\text{par}}-1} \eta_i \delta(\varphi - \varphi_i), \quad (13)$$

where  $\eta_i \in [0, 1]$  is the prior weight associated with the particle  $\varphi_i$ ,  $\sum_{i=0}^{N_{\text{par}}-1} \eta_i = 1$ , and  $\delta(\cdot)$  is the Dirac delta distribution. Then, under the Gibbs rule (12), the posterior distribution  $q(\varphi|\mathbf{y})$  given  $\mathbf{y}$  can be represented as

$$q(\varphi|\mathbf{y}) = \sum_{i=0}^{N_{\text{par}}-1} u_i \delta(\varphi - \varphi_i), \quad (14)$$

where  $u_i \in [0, 1]$  is the posterior weight associated with the particle  $\varphi_i$ ,  $\sum_{i=0}^{N_{\text{par}}-1} u_i = 1$ , and for every  $i \in [N_{\text{par}}]$ , we have

$$u_i \propto \eta_i e^{-\xi h(\mathbf{y}, \varphi_i)}. \quad (15)$$

*Example 1:* If the likelihood function can be exactly specified, i.e.,  $h(\mathbf{y}, \varphi) := -\ln q(\mathbf{y}|\varphi)$ , by setting  $\xi := 1$ , (15) particularizes to

$$u_i \propto \eta_i \cdot q(\mathbf{y}|\varphi_i) = \eta_i \cdot e^{-[-\ln q(\mathbf{y}|\varphi_i)]}, \quad (16)$$

which is the usual particle filter.  $\square$

Eqs. (13)–(15) form the foundation of our new particle filtering framework for signal-level target tracking. The enabling yet challenging step is to design a cost function  $h(\mathbf{y}, \varphi)$  without relying on the true likelihood function  $q(\mathbf{y}|\varphi)$ . In addition, this cost function satisfies the following rule.

*Rule 1:* At data  $\mathbf{y}$ , it holds that

$$h(\mathbf{y}, \varphi_1) \leq h(\mathbf{y}, \varphi_2), \quad (17)$$

or equivalently,

$$e^{-h(\mathbf{y}, \varphi_1)} \geq e^{-h(\mathbf{y}, \varphi_2)}, \quad (18)$$

if  $\varphi_1$  is preferred over  $\varphi_2$ .  $\square$

In line with Rule 1, this article suggests four concrete cost functions for PF-SLTR, which are conceptually simple and operationally manageable for MIMO radars. Other possibilities exist; however, they are to be identified by future research.

1) *Cost Functions in PF-SLTR*: The first two cost functions are motivated by the least-squares estimation.

*Method 1*: If we work with the time-domain signals in (4), we define

$$h_1(\mathbf{y}, \varphi) := \min_{\gamma \in \mathbb{C}} \sum_{p=0}^{N_p-1} \sum_{l=0}^{L-1} \left\| \mathbf{y}_p(l) - \gamma \mathbf{b}(\theta) \mathbf{a}^H(\theta) \mathbf{s}_p(l-\tau) e^{j2\pi p T_r \nu} \right\|_2^2, \quad (19)$$

where  $\mathbf{y}$  is a realized sample of the radar received signal  $\mathbf{y}_k$  in (6),  $\varphi := (\tau, \nu, \theta) \in \mathbb{R}^3$  is a hypothesized ToI-parameter vector, and  $\mathbf{y}_p(l)$  is a realized sample of  $\mathbf{y}_p(l)$  in (4).  $\square$

In  $h_1(\mathbf{y}, \varphi)$ , the nuisance parameter  $\gamma$  is marginalized out through the least-squares principle (i.e., the minimization operation). Different from Rao-Blackwellization, this operation can serve as an alternative approach to dimensionality reduction in particle filtering. The cost function  $h_1(\mathbf{y}, \varphi)$  can be computationally simplified.

*Proposition 1*: If the transmit array has the empirical spatial correlation  $\hat{\mathbf{R}}_s$ , then  $h_1(\mathbf{y}, \varphi)$  equals

$$h_1(\mathbf{y}, \varphi) = \sum_{p=0}^{N_p-1} \sum_{l=0}^{L-1} \mathbf{y}_p^H(l) \mathbf{y}_p(l) - \left| \sum_{p=0}^{N_p-1} \sum_{l=0}^{L-1} \mathbf{y}_p^H(l) \mathbf{b}(\theta) \mathbf{a}^H(\theta) \mathbf{s}_p(l-\tau) e^{j2\pi p T_r \nu} \right|^2 \quad (20)$$

where  $L_{ss}$  denotes the number of snapshots contained in the pulse  $\{\mathbf{s}_p(l)\}_{\forall l \in [L_{ss}]}$ , for every  $p \in [N_p]$ . When  $\hat{\mathbf{R}}_s = P_t \mathbf{I}_{N_t}$ , the denominator becomes  $P_t N_t N_r N_p L_{ss}$ , which is  $\varphi$ -independent.

*Proof*: See Appendix B.  $\square$

*Method 2*: If we work with the frequency-domain signals in (5), we define

$$h_2(\mathbf{y}, \varphi) := \min_{\gamma \in \mathbb{C}} \sum_{p=0}^{N_p-1} \sum_{n=0}^{N_{cr}-1} \left\| \bar{\mathbf{y}}_p(n) - \gamma \mathbf{b}(\theta) \mathbf{a}^H(\theta) \bar{\mathbf{s}}_p(n) e^{-j2\pi n \Delta \tau} e^{j2\pi p T_r \nu} \right\|_2^2, \quad (21)$$

where  $\mathbf{y}$  is a realized sample of the radar received signal  $\mathbf{y}_k$  in (6),  $\varphi := (\tau, \nu, \theta) \in \mathbb{R}^3$  is a hypothesized ToI-parameter vector, and  $\bar{\mathbf{y}}_p(n)$  is a realized sample of  $\bar{\mathbf{y}}_p(n)$  in (5).  $\square$

Due to the minimization operation over  $\gamma$ , by employing  $h_2(\mathbf{y}, \varphi)$ , dimensionality reduction in particle filtering is implicitly conducted; cf. Rao-Blackwellization. The cost function  $h_2(\mathbf{y}, \varphi)$  can be computationally simplified as follows.

*Proposition 2*: If the transmit array has the empirical spatial correlation  $\hat{\mathbf{R}}_s$ , then  $h_2(\mathbf{y}, \varphi)$  equals

$$h_2(\mathbf{y}, \varphi) = \sum_{p=0}^{N_p-1} \sum_{n=0}^{N_{cr}-1} \bar{\mathbf{y}}_p^H(n) \bar{\mathbf{y}}_p(n) - \left| \sum_{p=0}^{N_p-1} \sum_{n=0}^{N_{cr}-1} \bar{\mathbf{y}}_p^H(n) \mathbf{b}(\theta) \mathbf{a}^H(\theta) \bar{\mathbf{s}}_p(n) e^{-j2\pi n \Delta \tau} e^{j2\pi p T_r \nu} \right|^2 \quad (22)$$

where  $N_{cr}$  denotes the number of frequency bins (i.e., FFT points) to represent  $\{\bar{\mathbf{s}}_p(n)\}_{\forall n \in [N_{cr}]}$ , for every  $p \in [N_p]$ . When  $\hat{\mathbf{R}}_s = P_t \mathbf{I}_{N_t}$ , the denominator in the second line becomes  $P_t N_t N_r N_p N_{cr}$ , which is  $\varphi$ -independent.

*Proof*: Similar to the proof of Proposition 1.  $\square$

As we can see from Propositions 1 and 2, to expect small values of  $h_1(\mathbf{y}, \varphi)$  and  $h_2(\mathbf{y}, \varphi)$  when given  $\mathbf{y}$ , it suffices to have large values for the numerators in (20) and (22), respectively, if  $\hat{\mathbf{R}}_s = P_t \mathbf{I}_{N_t}$ . The two numerators are exactly the ambiguity functions (i.e., the matched filters) for pulsed multi-carrier MIMO radars in the time domain and frequency domain, respectively [19, Eq. (33)], [64, p. 131]. The next two cost functions are inspired by this observation.

*Method 3*: If we work with the time-domain signals in (4), we define

$$h_3(\mathbf{y}, \varphi) := -\ln \left[ \sum_{p=0}^{N_p-1} \sum_{l=0}^{L-1} \mathbf{y}_p^H(l) \mathbf{b}(\theta) \mathbf{a}^H(\theta) \mathbf{s}_p(l-\tau) e^{j2\pi p T_r \nu} \right]^2, \quad (23)$$

where  $\mathbf{y}$  is a realized sample of the radar received signal  $\mathbf{y}_k$  in (6),  $\varphi := (\tau, \nu, \theta) \in \mathbb{R}^3$  is a hypothesized ToI-parameter vector, and  $\mathbf{y}_p(l)$  is a realized sample of  $\mathbf{y}_p(l)$  in (4).  $\square$

Note that the  $|\cdot|^2$  term, i.e., the argument of the  $-\ln$  function, in (23) is the empirical matched filter in the time domain. Using Method 3, (15) becomes

$$u_i \propto \eta_i \cdot \left| \sum_{p=0}^{N_p-1} \sum_{l=0}^{L-1} \mathbf{y}_p^H(l) \mathbf{b}(\theta_i) \mathbf{a}^H(\theta_i) \mathbf{s}_p(l-\tau_i) e^{j2\pi p T_r \nu_i} \right|^2, \quad (24)$$

where  $(\tau_i, \nu_i, \theta_i)$  denotes the  $i^{\text{th}}$  particle. Eq. (24) aligns well with our intuition because, the closer the parameter pair  $(\tau_i, \nu_i, \theta_i)$  is to its true value  $(\tau_0, \nu_0, \theta_0)$ , the larger the value of the ambiguity function evaluated at  $(\tau_i, \nu_i, \theta_i)$ , and thus the more the collected radar data  $\mathbf{y}$  supports the particle  $(\tau_i, \nu_i, \theta_i)$ .

*Method 4*: If we work with the frequency-domain signals in (5), we define

$$h_4(\mathbf{y}, \varphi) := -\ln \left[ \sum_{p=0}^{N_p-1} \sum_{n=0}^{N_{cr}-1} \left| \bar{\mathbf{y}}_p^H(n) \mathbf{b}(\theta) \mathbf{a}^H(\theta) \bar{\mathbf{s}}_p(n) e^{-j2\pi n \Delta \tau} e^{j2\pi p T_r \nu} \right|^2 \right], \quad (25)$$

where  $\mathbf{y}$  is a realized sample of the radar received signal  $\mathbf{y}_k$  in (6),  $\varphi := (\tau, \nu, \theta) \in \mathbb{R}^3$  is a hypothesized ToI-parameter vector, and  $\bar{\mathbf{y}}_p(n)$  is a realized sample of  $\bar{\mathbf{y}}_p(n)$  in (5).  $\square$

Note that the  $|\cdot|^2$  term, i.e., the argument of the  $-\ln$  function, in (25) is the empirical matched filter in the frequency domain. Using Method 4, (15) becomes

$$u_i \propto \eta_i \cdot \left| \sum_{p=0}^{N_p-1} \sum_{n=0}^{N_{cr}-1} \bar{\mathbf{y}}_p^H(n) \mathbf{b}(\theta_i) \mathbf{a}^H(\theta_i) \bar{\mathbf{s}}_p(n) e^{-j2\pi n \Delta \tau_i} e^{j2\pi p T_r \nu_i} \right|^2, \quad (26)$$

where  $(\tau_i, \nu_i, \theta_i)$  denotes the  $i^{\text{th}}$  particle. Again, the closer the parameter pair  $(\tau_i, \nu_i, \theta_i)$  is to its true value  $(\tau_0, \nu_0, \theta_0)$ , the larger the value of the ambiguity function evaluated at  $(\tau_i, \nu_i, \theta_i)$ , and thus the more the collected radar data  $\mathbf{y}$  supports the particle  $(\tau_i, \nu_i, \theta_i)$ .

The cost functions  $h_3(\mathbf{y}, \varphi)$  and  $h_4(\mathbf{y}, \varphi)$  are conceptually comply with  $h_1(\mathbf{y}, \varphi)$  and  $h_2(\mathbf{y}, \varphi)$ ; cf. Propositions 1 and 2. However,  $h_3(\mathbf{y}, \varphi)$  and  $h_4(\mathbf{y}, \varphi)$  are computationally more lightweight than  $h_1(\mathbf{y}, \varphi)$  and  $h_2(\mathbf{y}, \varphi)$ , especially when implementing the Gibbs-posterior-based PF-SLTR; see (24) and (26). To limit the computational complexity, hereafter, this article focuses on the cost functions  $h_3(\mathbf{y}, \varphi)$  and  $h_4(\mathbf{y}, \varphi)$ . The cost functions  $h_1(\mathbf{y}, \varphi)$  and  $h_2(\mathbf{y}, \varphi)$  in this article are more analytically motivational than practically instructive; note that  $h_1(\mathbf{y}, \varphi)$  and  $h_2(\mathbf{y}, \varphi)$  motivate the proposals of  $h_3(\mathbf{y}, \varphi)$  and  $h_4(\mathbf{y}, \varphi)$ , respectively.

2) *Property Analysis*: In this subsection, we analyze the properties of the proposed cost functions. As elucidated before, we are particularly interested in  $h_3(\mathbf{y}, \varphi)$  and  $h_4(\mathbf{y}, \varphi)$  for their computational advantages. Since  $h_3(\mathbf{y}, \varphi)$  and  $h_4(\mathbf{y}, \varphi)$  are mathematically equivalent under FFT and inverse FFT (IFFT), it suffices to analyze the property of  $h_4(\mathbf{y}, \varphi)$  only. The proposition below shows that  $h_4(\mathbf{y}, \varphi)$  aligns with Rule 1 in a well-specified tracking gate. A tracking gate (or validation gate) is a hypothesized region in which the target is assumed to be located; that is, it is a delimited subspace of  $\mathbb{R}^3$  in which the true target parameters  $(\tau_0, \nu_0, \theta_0)$  are included.

*Proposition 3*: Suppose that the transmitted signals are spatially uncorrelated with  $\mathbf{R}_s := \mathbb{E}\bar{\mathbf{s}}_p(n)\bar{\mathbf{s}}_p^H(n) = P_t \mathbf{I}_{N_t}$ , for every  $p \in [N_p]$  and  $n \in [N_{\text{cr}}]$ , and there are no scatterers, i.e.,  $N_s := 0$  in (2). Additionally, we suppose that the transmitter and the receiver are uniform linear arrays with half-wavelength spacing: that is,

$$\mathbf{a}(\theta) := [1, e^{-j\pi \sin \theta}, \dots, e^{-j\pi(N_t-1) \sin \theta}]^T, \quad (27)$$

and

$$\mathbf{b}(\theta) := [1, e^{-j\pi \sin \theta}, \dots, e^{-j\pi(N_r-1) \sin \theta}]^T. \quad (28)$$

Let  $N_{tr} := \max\{N_t, N_r\}$ . Then, within the tracking gate

$$\begin{aligned} & \left[ \tau_0 - \frac{1}{B}, \tau_0 + \frac{1}{B} \right] \times \left[ \nu_0 - \frac{1}{T_i}, \nu_0 + \frac{1}{T_i} \right] \times \\ & \left[ \arcsin \left( \sin \theta_0 - \frac{2}{N_{tr}} \right), \arcsin \left( \sin \theta_0 + \frac{2}{N_{tr}} \right) \right], \end{aligned} \quad (29)$$

the cost function

$$-\ln \left[ \left| \sum_{p=0}^{N_p-1} \sum_{n=0}^{N_{\text{cr}}-1} \mathbb{E}_{\bar{\mathbf{y}}_p(n), \bar{\mathbf{s}}_p(n)} \left[ \right. \right. \right. \begin{aligned} & \left. \left. \left. \mathbf{y}_p^H(n) \mathbf{b}(\theta) \mathbf{a}^H(\theta) \bar{\mathbf{s}}_p(n) e^{-j2\pi n \Delta \tau} e^{j2\pi p T_r \nu} \right] \right|^2 \right], \quad (30)$$

induced by  $h_4(\mathbf{y}, \varphi)$  in (25), through inner-expectation over  $\bar{\mathbf{y}}_p(n)$  and  $\bar{\mathbf{s}}_p(n)$ , satisfies Rule 1.

*Proof*: See Appendix C.  $\square$

Due to the randomness of  $\bar{\mathbf{y}}_p(n)$  and  $\bar{\mathbf{s}}_p(n)$  in (25), we resort to the expected version in (30) for property analysis, to be specific, the analysis on the statistical property instead of the single-sample property. In the practice of PF-SLTR,

however, (25) should be used to update the weights of the particles; see (26). When  $\mathbf{R}_s$ ,  $\mathbf{a}$ , and  $\mathbf{b}$  are specified by other more complicated values, the tracking gate has to be calculated differently. When  $N_s$  is nonzero, we suppose that scatterers are well-separated from the ToI so the interference can be negligible within the specified tracking gate.

Next, we investigate the role of the parameter  $\xi$  in (24) and (26). Let  $\boldsymbol{\alpha} := [\alpha_0, \alpha_1, \dots, \alpha_{N_{\text{par}}-1}] > 0$  denote a non-degenerate  $N_{\text{par}}$ -dimensional discrete probability vector, summing to unity. Taking (24) as an example, we can define

$$\alpha_i \propto \left| \sum_{p=0}^{N_p-1} \sum_{l=0}^{L-1} \mathbf{y}_p^H(l) \mathbf{b}(\theta_i) \mathbf{a}^H(\theta_i) \mathbf{s}_p(l - \tau_i) e^{j2\pi p T_r \nu_i} \right|^2,$$

resulting in the following rule for generating posterior weights:

$$u_i \propto \eta_i \alpha_i^\xi, \quad \forall i \in [N_{\text{par}}].$$

Let  $\boldsymbol{\alpha}^{(\xi)} := [\alpha_0^\xi, \alpha_1^\xi, \dots, \alpha_{N_{\text{par}}-1}^\xi] / C_\xi$  denote a new distribution powered by  $\xi \geq 0$  from  $\boldsymbol{\alpha}$ , where  $C_\xi := \sum_{i=0}^{N_{\text{par}}-1} \alpha_i^\xi$  is the normalization factor. We have the following result regarding the entropy values of  $\boldsymbol{\alpha}$  and  $\boldsymbol{\alpha}^{(\xi)}$ .

*Theorem 1*: It holds that

$$-\sum_{i=0}^{N_{\text{par}}-1} \alpha_i \ln \alpha_i \begin{cases} \leq -\sum_{i=0}^{N_{\text{par}}-1} \alpha_i^{(\xi)} \ln \alpha_i^{(\xi)}, & \text{if } 0 \leq \xi \leq 1; \\ \geq -\sum_{i=0}^{N_{\text{par}}-1} \alpha_i^{(\xi)} \ln \alpha_i^{(\xi)}, & \text{if } \xi \geq 1. \end{cases}$$

*Proof*: See Appendix D, where it shows that the entropy function  $\xi \mapsto -\sum_{i=0}^{N_{\text{par}}-1} \alpha_i^{(\xi)} \ln \alpha_i^{(\xi)}$  is monotonically decreasing in  $\xi \geq 0$ .  $\square$

Theorem 1 implies that when  $0 \leq \xi \leq 1$ , we make the  $\mathbf{y}$ -data evidence (i.e., likelihood values  $\{\alpha_i\}_{i \in [N_{\text{par}}]}$ ) more balanced across all particles  $\{\mathbf{x}_i\}_{i \in [N_{\text{par}}]}$ ; when  $\xi \geq 1$ , we let the  $\mathbf{y}$ -data evidence be more concentrated on particles that have large likelihoods. An illustrative example is given below.

*Example 2*: Let  $\boldsymbol{\alpha} := [0.2, 0.5, 0.3]$ . If  $\xi = 0.5$ , we have  $\boldsymbol{\alpha}^{(0.5)} = [0.2628, 0.4154, 0.3218]$ ; if  $\xi = 2$ , we have  $\boldsymbol{\alpha}^{(2)} = [0.1053, 0.6579, 0.2368]$ . As indicated,  $\boldsymbol{\alpha}^{(0.5)}$  is more balanced (i.e., having smaller differences) than  $\boldsymbol{\alpha}$ , while  $\boldsymbol{\alpha}^{(2)}$  is more polarized (i.e., having larger differences) than  $\boldsymbol{\alpha}$ .  $\square$

In the context of particle filtering, balanced prior and likelihood weights lead to balanced posterior weights, which in turn can benefit combating particle degeneracy, provided that particles are diverse and informative. In particle filtering, to ensure diversity and informativity, particles should be drawn from a well-designed proposal distribution [37, pp. 178-180].

#### IV. MIMO-OFDM INTEGRATED SENSING AND COMMUNICATIONS: PF-SLTR

The proposed time structure of OFDM ISAC waveforms for PF-SLTR is shown in Fig. 1, which applies to every transmit antenna in MIMO. A target tracking period  $T_t$ , which is usually in dozens of milliseconds (ms; e.g., 25ms, 50ms), contains one ISAC period  $T_i$  to sense the moving ToI. Tens or hundreds of microseconds ( $\mu\text{s}$ ) are, in practice, sufficient for an ISAC period. To save computing resources and without

compromising the necessary accuracy of target tracking, there is no need to use the entire  $T_t$  time window for radar sensing. The remaining  $T_t - T_i$  seconds can be completely designed for pure communications to improve, e.g., throughput and reliability. Depending on how we use an MIMO-OFDM ISAC station, we can employ two types of waveform structures:

- **Pulsed Waveforms:** In this scheme, silent times are included between consecutive pulses. The transmit array and the radar receive array operate in either a time-division duplex or full-duplex manner, corresponding to the non-blind minimum round-trip delay of  $T_p$  or 0, respectively. During these silent times, the radar receiver can listen to *far* target echoes and resolves target parameters. This scheme is identical to that of the typical pulse-Doppler radars, and the maximum detectable range is determined by the duration of the silence, i.e.,  $T_r - T_p$ , where  $T_p$  is the pulse duration and  $T_r$  is the pulse repetition interval. Within each pulse duration, several OFDM symbols, together with their cyclic prefixes (CPs), are arranged back-to-back. This is a *sensing-centric* solution where the ranging capacity is improved by adding silent times and sacrificing the communications throughput.
- **Continuous-Wave (CW) Waveforms:** In this scheme, no silent times are contained between consecutive pulses. The transmit array and the radar receive array are supposed to be well isolated, and they operate in a full-duplex manner. The maximum resolvable range is determined by the length of the CP, which ensures that the *near* ToI can be treated as a scatterer. As a result, the CP length fully covers all possible path delays so that the circular convolution property is preserved for FFT-based signal processing, for example, frequency-domain channel estimation for communications and matched filtering for ranging. This is a *communications-centric* solution where the CP duration limits the ranging capacity, while the communication data streams remain unaffected.

Note that in the pulsed case, the circular convolution property is not inherently preserved for sensing signal processing, because the ToI, as a scatterer in the sensing channel, may not fall within the CP duration. Therefore, FFT-based frequency-domain methods require additional treatment compared to the CW case, as to be elaborated on in the following subsections. However, the scattering effect of the ToI may not impact the communication channel, since in the pulsed case, targets are typically far from the station, whereas communication users are located much closer. If the sensing ToI and communication users are both nearby, the CW scheme—where the CP can cover all path delays—should be adopted.

#### A. Pulsed MIMO-OFDM ISAC

In this mode, MIMO-OFDM ISAC works like a pulsed radar, and the only distinction is that the OFDM waveforms are employed at transmit antennas, instead of the canonical radar waveforms (e.g., phase-coded and chirp signals). Suppose that  $M$  OFDM symbols are included in each pulse, and the number of subcarriers in OFDM is  $N_c$ . We have  $T_p = M \cdot (T_c + T_o)$  and  $T_o = 1/\Delta_f = N_c/B = N_c T_s$ , where  $\Delta_f$  is the subcarrier

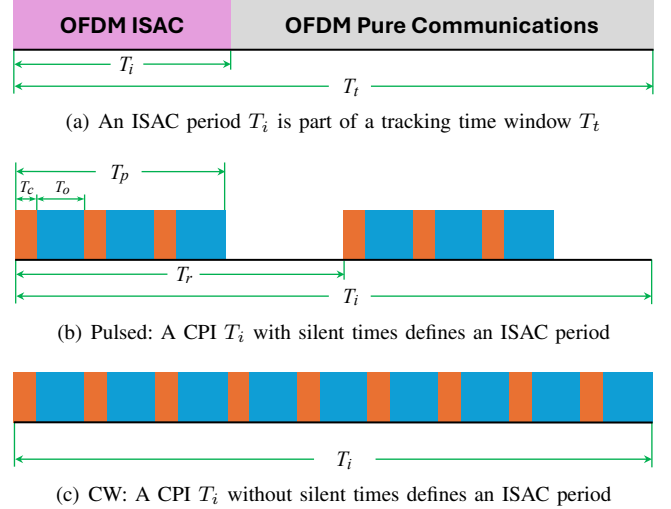


Fig. 1. The time structure of OFDM ISAC waveforms. Cyclic prefixes (CPs) are visualized by orange rectangles, while data payloads are indicated by blue rectangles. (b): pulsed OFDM ISAC waveforms; (c): continuous-wave (CW) OFDM ISAC waveforms. The tracking time period is  $T_t$ , and the ISAC period is  $T_i$ . For pulsed waveforms in (b), within a coherent processing interval (CPI)  $T_i$ , two pulses repeat with the pulse repetition interval (PRI)  $T_r$ . Each pulse has the time duration  $T_p$ . The silent time between two consecutive pulses is therefore  $T_r - T_p$ . Within each pulse, three CP-appended OFDM symbols are included; the duration of each OFDM symbol is  $T_o$ , whereas that of each CP is  $T_c$ . For CW waveforms in (c), we can treat  $T_r = T_p$  so that no silent times are inserted. The Doppler processing for both structures is algorithmically similar. The maximum detectable range for the pulsed case is determined by the silence time through  $C \cdot (T_r - T_p)/2$ , while that for the CW case is by the CP duration through  $CT_c/2$ .

spacing. Let  $\mathbf{c}_{p,m}(n) \in \mathbb{C}^{N_t}$  denote the constellation points on the  $n^{\text{th}}$  subcarrier in the  $p^{\text{th}}$  pulse and  $m^{\text{th}}$  OFDM symbol, where  $p \in [N_p]$ ,  $m \in [M]$ , and  $n \in [N_c]$ . The time-domain waveform  $\mathbf{s}_p(l)$  to be transmitted in the  $p^{\text{th}}$  pulse is

$$\mathbf{s}_p(l) = \begin{cases} \mathbf{s}_{p,\text{eff}}(l), & \text{if } 0 \leq l \leq \langle T_p/T_s \rangle, \\ \mathbf{0}, & \text{if } \langle T_p/T_s \rangle + 1 \leq l \leq \langle T_r/T_s \rangle, \end{cases} \quad (31)$$

where  $\mathbf{s}_{p,\text{eff}}(l)$  for  $0 \leq l T_s \leq T_p$  is the effective (i.e., non-zero) transmit waveform at the logical time  $l$  in the  $p^{\text{th}}$  pulse, consisting of  $M$  back-to-back CP-appended OFDM time-domain symbols;  $\{\mathbf{s}_{p,\text{eff}}(l)\}_{l: 0 \leq l \leq \langle T_p/T_s \rangle}$  is determined by  $\{\mathbf{c}_{p,m}(n)\}_{\forall p \in [N_p], m \in [M], n \in [N_c]}$  via IFFT and CP addition; see, e.g., [14, Eq. (3)], [15, Eq. (2)], [13, Eq. (1)]. Note that within the time window  $[T_p, T_r]$ , the transmitter keeps silent. Note also that  $N_{\text{cr}} \neq N_c$ : the former is the FFT length of the whole transmit signal  $\{\mathbf{s}_p(l)\}_{\forall l \in [L]}$  in which multiple CP-added OFDM symbols and a silent time slot are contained [cf. (5) and (25)], while the latter is the FFT length of one single CP-excluded OFDM symbol. In the practice of pulsed radars,  $N_c \ll N_{\text{cr}} = L$ .

The transmit MIMO-OFDM time-domain signals  $\mathbf{s}_p$  defined in (31) are then propagated through the MIMO channel (4) and received by the radar receive array as  $\{\mathbf{y}_p(l)\}_{\forall l \in [L]}$ . The data evidence for a hypothesized ToI parameter pair  $\varphi := (\tau, \nu, \theta) \in \mathbb{R}^3$  is quantified by the cost functions in Methods 1 and 3, to be fed into the Gibbs-posterior-based PF-SLTR (15). If frequency-domain Methods 2 and 4 are to be used, FFT from  $\{\mathbf{s}_p(l)\}_{\forall l \in [L]}$  to  $\{\bar{\mathbf{s}}_p(n)\}_{\forall n \in [N_{\text{cr}}]}$

must be explicitly conducted *without removing CPs*, because the circular convolution property of FFT was destroyed, so that CPs are also part of effective sensing waveforms and  $\{\bar{\mathbf{s}}_p(n)\}_{\forall n \in [N_{\text{cr}}]}$  do not equal to  $\{\mathbf{c}_{p,m}(n)\}_{\forall m \in [M], n \in [N_c]}$ .

### B. Continuous-Wave MIMO-OFDM ISAC

The pulse-Doppler radar signal processing can also be applied to CW MIMO-OFDM ISAC systems, just treating  $T_r = T_p = M \cdot (T_c + T_o)$ . Because we assumed that the maximum target round-trip delay is covered by the CP duration, the circular convolution property of the FFT can be preserved. As a result, efficient frequency-domain processing is applicable. To be specific, *after CP removal*, the MIMO channel propagation can be written as

$$\bar{\mathbf{y}}_{p,m}(n) = \beta_0 \mathbf{b}(\theta_0) \mathbf{a}^H(\theta_0) \mathbf{c}_{p,m}(n) e^{-j2\pi n \Delta_f \tau_0} e^{j2\pi p T_r \nu_0} + \bar{\mathbf{n}}_{c,p,m}(n), \quad (32)$$

for every  $p \in [N_p]$ ,  $m \in [M]$ , and  $n \in [N_c]$  (not  $[N_{\text{cr}}]$ ). Note that within the same pulse, the Doppler frequency shift is assumed to be constant so that the Doppler phase term  $e^{j2\pi p T_r \nu_0}$  does not depend on  $m$ . Therefore, the data evidence for a hypothesized ToI parameter pair  $\varphi := (\tau, \nu, \theta) \in \mathbb{R}^3$  is quantified by the cost functions in frequency-domain Methods 2 and 4. Note that  $h_2$  and  $h_4$  need to be slightly modified to encompass the summations over  $m \in [M]$  and  $n \in [N_c]$ :

$$h'_2(\mathbf{y}, \varphi) := \min_{\gamma \in \mathbb{C}} \sum_{p=0}^{N_p-1} \sum_{m=0}^{M-1} \sum_{n=0}^{N_c-1} \left\| \bar{\mathbf{y}}_{p,m}(n) - \gamma \mathbf{b}(\theta) \mathbf{a}^H(\theta) \mathbf{c}_{p,m}(n) e^{-j2\pi n \Delta_f \tau} e^{j2\pi p T_r \nu} \right\|_2^2, \quad (33)$$

and

$$h'_4(\mathbf{y}, \varphi) := -\ln \left[ \left| \sum_{p=0}^{N_p-1} \sum_{m=0}^{M-1} \sum_{n=0}^{N_c-1} \bar{\mathbf{y}}_{p,m}^H(n) \mathbf{b}(\theta) \mathbf{a}^H(\theta) \mathbf{c}_{p,m}(n) e^{-j2\pi n \Delta_f \tau} e^{j2\pi p T_r \nu} \right|^2 \right]. \quad (34)$$

Numerically evaluating (33) and (34) in the frequency domain, especially when the FFT technique is applied, can be significantly faster than evaluating (19) and (23) in the time domain. This highlights the computational benefit of the CW MIMO-OFDM ISAC systems, however, coming with a limited ranging capability set by the CP duration. In contrast, pulsed MIMO-OFDM ISAC systems can support much larger ranging regions without considering the time length of CPs, however, at the cost of a higher computational burden<sup>2</sup> and lower communications throughput.

### C. Overall PF-SLTR Algorithm

In this section, we summarize the PF-SLTR for MIMO-OFDM ISAC systems in Algorithm 1, which is adapted from the canonical particle filter for dynamic systems (1); see [37, Algorithm 4], [38, p. 468]. Some algorithmic details and

<sup>2</sup>Although this burden can be algorithmically reduced by FFT tricks; cf. (23) and (25); NB: in practice,  $MN_c \leq N_{\text{cr}}$  and  $N_c \ll N_{\text{cr}}$ .

operational remarks, such as the basics of particle filtering and the notions of resampling and effective sample size, can be seen in [37], [38, Chap. 15], [39].

---

#### Algorithm 1 PF-SLTR in MIMO-OFDM ISAC

---

**Definition:**  $k$  is the discrete tracking-time index;  $N_{\text{par}}$  is the number of state particles;  $\mathbf{x}_{k,i}$  is the posterior state particles at  $k$  and  $u_{k,i}$  the associated weights,  $\forall i \in [N_{\text{par}}]$ ;  $\varphi_{k,i}$  is the range-Doppler-angle representation of  $\mathbf{x}_{k,i}$ ;  $N_{\text{eff}}$  is the effective sample size and  $N_{\text{thres}}$  its threshold.

**Remark:** For illustration and computational efficiency, we only show frequency-domain processing using (25) and (34). In addition, we suppose that the waveforms at transmit antennas are uncorrelated, i.e.,  $\hat{\mathbf{R}}_s := P_t \mathbf{I}_{N_t}$ ; otherwise, cost functions can be modified by incorporating denominators as in Propositions 1 and 2.

**Initialization:**  $N_{\text{par}}$ ,  $N_{\text{thres}}$ ,  $\xi$ , and  $\{\mathbf{x}_{0,i}, u_{0,i}\}_{i \in [N]}$ .

**Input:** Radar received signals  $\mathbf{y}_k$ ,  $k = 1, 2, 3, \dots$ ; see (6)

```

1: // Step 1: Generate Prior State Particles; See (1)
2: for  $i = 0 : N_{\text{par}} - 1$  do
3:   Sample  $\mathbf{w}_{k-1,i}$  from the distribution of  $\mathbf{w}_{k-1}$ 
4:    $\mathbf{x}_{k,i} = \mathbf{f}_k(\mathbf{x}_{k-1,i}, \mathbf{w}_{k-1,i})$ 
5:   Translate  $\mathbf{x}_{k,i}$  to  $\varphi_{k,i}$  using geometric relations
6:    $\eta_{k,i} \leftarrow u_{k-1,i}$ 
7: end for
8: // Step 2: Evaluate  $\mathbf{y}_k$ -Data Evidence for Every  $\varphi_{k,i}$ 
9: for  $i = 0 : N_{\text{par}} - 1$  do
10:  if Pulsed Scheme then
11:    Calculate cost  $h(\mathbf{y}_k, \varphi_{k,i})$  using (25)
12:  else if CW Scheme then
13:    Calculate cost  $h(\mathbf{y}_k, \varphi_{k,i})$  using (34)
14:  end if
15: end for
16: // Step 3: Generate Posterior Particles  $\mathbf{x}_{k,i}$ ; See (15)
17: for  $i = 0 : N_{\text{par}} - 1$  do
18:  Keep  $\mathbf{x}_{k,i}$  unchanged
19:  Update weight by  $u_{k,i} \leftarrow \eta_{k,i} \cdot e^{-\xi h(\mathbf{y}_k, \varphi_{k,i})}$ 
20: end for
21: Normalize weights  $\{u_{k,i}\}_{\forall i \in [N_{\text{par}}]}$ 
22: // Step 4: Resampling
23:  $N_{\text{eff}} \leftarrow 1 / \sum_{i=0}^{N_{\text{par}}-1} u_{k,i}$ 
24: if  $N_{\text{eff}} < N_{\text{thres}}$  then
25:  Resample  $N_{\text{par}}$  times from  $\{\mathbf{x}_{k,i}, u_{k,i}\}_{\forall i \in [N_{\text{par}}]}$ 
26:   $u_{k,i} \leftarrow 1/N_{\text{par}}, \forall i \in [N_{\text{par}}]$ 
27: end if

```

**Output:** Posterior particles and weights  $\{\mathbf{x}_{k,i}, u_{k,i}\}_{\forall i \in [N_{\text{par}}]}$ .

---

The computational complexity, in time, of PF-SLTR can be analyzed as follows:

- In Step 1, if  $\mathbf{f}_k$  is linear in  $\mathbf{x}_{k-1}$ , which is the case for the usual constant-velocity and constant-acceleration models [35], the complexity is  $\mathcal{O}(N_{\text{par}} d_x^2)$ , where  $d_x$  denotes the dimension of  $\mathbf{x}_{k-1}$  (assuming fixed across different  $k$ 's).
- In Step 2, for the pulsed scheme, the complexity is  $\mathcal{O}(N_{\text{par}} N_p N_{\text{cr}} (N_t + \hat{N}_r))$ ; for the CW scheme, the complexity is  $\mathcal{O}(N_{\text{par}} N_p M N_c (N_t + N_r))$ .

- In Step 3, the complexity is  $\mathcal{O}(N_{\text{par}})$  because the  $\mathbf{y}_k$ -data evidence  $\{h(\mathbf{y}_k, \varphi_{k,i})\}_{\forall i \in [N_{\text{par}}]}$  of the particles have already been evaluated in Step 2.
- In Step 4, the complexity is  $\mathcal{O}(N_{\text{par}})$ , if the systematic resampling is adopted.

Overall, the computational complexity in time of PF-SLTR is  $\mathcal{O}(N_{\text{par}}d_x^2 + N_{\text{par}}N_pN_{\text{cr}}(N_t + N_r))$  for the pulsed scheme, and is  $\mathcal{O}(N_{\text{par}}d_x^2 + N_{\text{par}}N_pMN_c(N_t + N_r))$  for the CW scheme.

## V. EXPERIMENTS

In this section, we use experiments to validate the efficiency of the proposed PF-SLTR (i.e., Algorithm 1) in MIMO-OFDM ISAC systems. Suppose that the state vector  $\mathbf{x}_k$  contains the ToI parameters  $\varphi_k = (\tau_{0,k}, \nu_{0,k}, \theta_{0,k})$  in radar's polar coordinate. For the state transition equation  $\mathbf{x}_k = \mathbf{f}_k(\mathbf{x}_{k-1}, \mathbf{w}_{k-1})$  in (1), we use the constant-velocity (CV) model [43] because within every coherent processing interval, the range-Doppler-angle parameters of the ToI are assumed to remain unchanged. The following three particle filtering schemes are implemented for performance comparison.

- PF-ILTR: The traditional particle filtering (PF) for information-level target tracking (ILTR). First, we obtain the measurements of  $(\tau_0, \nu_0, \theta_0)$  at each tracking time  $k$ , using the 3-dimensional (3D) range-Doppler-DoA matched filter. For demonstration purposes only, other advanced methods, e.g., [16], [25], [26], [49, Table II], are not implemented because they are even more computationally prohibitive for real-time use (e.g., within the tracking time window  $T_t = 50\text{ms}$ ). The computational complexity, in time, of the 3D range-Doppler-DoA matched filters (25) and (34) is  $\mathcal{O}(N_{\text{tg}}^3 N_p N_{\text{cr}}(N_t + N_r))$  and  $\mathcal{O}(N_{\text{tg}}^3 N_p M N_c(N_t + N_r))$ , respectively, where  $N_{\text{tg}}$  is the length of the tracking gate in each dimension. To clarify, to search for the peak of the matched filter output in a  $N_{\text{tg}} \times N_{\text{tg}} \times N_{\text{tg}}$  grid of range-Doppler-DoA, we need to evaluate the ambiguity function (25) or (34)  $N_{\text{tg}}^3$  times. As indicated, even  $N_{\text{tg}} = 30$ , we need to evaluate ambiguity functions 27000 times, and the complexity of each time is  $\mathcal{O}(N_p N_{\text{cr}}(N_t + N_r))$  or  $\mathcal{O}(N_p M N_c(N_t + N_r))$ . For systems with large  $N_p$ ,  $N_{\text{cr}}$  (i.e.,  $L$ ,  $M$ ,  $N_c$ ,  $N_t$ , and  $N_r$ ), even the traditional 3D range-Doppler-DoA matched filtering is unaffordable, no mention advanced approaches [25], [26], [49, Table II].
- PF-SLTR-A: The traditional particle filtering (PF) for signal-level target tracking (SLTR) that augments (A) the real and imaginary components of the complex gain  $\beta_0$  (due to the DoI) into the state vector  $\mathbf{x}_k$  [36], [40], [41]. It is assumed that the conditional distribution  $q(\mathbf{y}_k | \mathbf{x}_k)$  is complex Gaussian and there are no scatterers. To be specific, at the tracking time  $k$ , for every  $p, m, n$ , we have

$$q(\bar{\mathbf{y}}_{k,p}(n) | \beta_0, \tau_0, \nu_0, \theta_0) \sim \mathcal{CN}(\epsilon_1, \sigma_{\text{cn}}^2 \mathbf{I}_{N_r}) \quad (35)$$

where  $\epsilon_1 := \beta_0 \mathbf{b}(\theta_0) \mathbf{a}^H(\theta_0) \bar{\mathbf{s}}_p(n) e^{-j2\pi n \Delta \tau_0} e^{j2\pi p T_r \nu_0}$ , for the pulsed MIMO-OFDM paradigm [see (5)], or

$$q(\bar{\mathbf{y}}_{k,p,m}(n) | \beta_0, \tau_0, \nu_0, \theta_0) \sim \mathcal{CN}(\epsilon_2, \sigma_{\text{cn}}^2 \mathbf{I}_{N_r}) \quad (36)$$

where  $\epsilon_2 := \beta_0 \mathbf{b}(\theta_0) \mathbf{a}^H(\theta_0) \mathbf{c}_{p,m}(n) e^{-j2\pi n \Delta_f \tau_0} e^{j2\pi p T_r \nu_0}$  for the CW MIMO-OFDM paradigm [see (32)];

$\mathcal{CN}(\epsilon, \sigma_{\text{cn}}^2 \mathbf{I}_{N_r})$  denotes the complex Gaussian distribution with mean  $\epsilon$ , covariance  $\sigma_{\text{cn}}^2 \mathbf{I}_{N_r}$ , and zero pseudo-covariance;  $\sigma_{\text{cn}}^2$  is the assumed-known power of the channel noise. The SNR of the system is therefore defined as  $10 \log_{10}(P_t / \sigma_{\text{cn}}^2)$ . As is frequently observed in practice, the convergence of PF-SLTR-A is difficult to ensure, especially when the path gain  $\beta_{k,0}$  is significantly time-varying across different  $k$ 's or when scatterers exist, which makes the likelihoods in (35) and (36) largely unreliable.

- RBPF-SLTR-A: The Rao-Blackwellized particle filtering (RBPF) [52] for signal-level target tracking (SLTR) that augments (A) the real and imaginary components of the complex gain  $\beta_{k,0}$  into the state vector  $\mathbf{x}_k$ . Since the station transition equation is linear in  $\mathbf{x}_{k-1}$  (due to the adoption of the CV model) and the measurement equation (2) [cf. (4) and (5)] is linear in  $\beta_{k,0}$ , the RBPF that marginalizes out  $\beta_{k,0}$  using a Kalman filter can improve the statistical and computational efficiency, compared to the traditional PF-SLTR-A; see [53, Sec. II-G].

The performance of each method is measured by both the running times and the target-tracking mean-squared errors (MSEs). The experiments were performed in MATLAB R2023a on an HP desktop with a 12th Gen Intel® Core™ i7-12700K processor (3.60 GHz), 64 GB of RAM, and a 64-bit operating system. All the source data and codes are available online at GitHub: <https://github.com/Spratm-Asleaf/PF-SLTR-MIMO-OFDM>.

We consider a continuous-wave MIMO-OFDM ISAC system with center frequency  $f_c = 10\text{GHz}$  for tracking a near and slow ToI. (Under the pulsed case for far and fast targets, the empirical claims in this subsection remain the same, which can be verified using shared source codes on GitHub.) The ToI is moving along a curved trajectory; see Fig. 2. In this case, the communication-centric waveform structure in Fig. 1(c) is used, and the cost function in (34) is employed in PF-SLTR to track the ToI. On the communications side, we suppose that each OFDM subcarrier contains random symbols uniformly from the quadrature amplitude modulation (QAM) constellation of order 64.

On the sensing side, the tracking time period is set to  $T_t = 50\text{ms}$ , and the total tracking time is 100s. To cover the maximum range of 150m, we let the CP duration be  $T_c = 1\mu\text{s}$ . Suppose that the OFDM symbol duration (for data payloads) is five times of the CP length (i.e.,  $T_o = 5\mu\text{s}$ ), the number of OFDM symbols in a pulse is  $M = 1$ , the number of subcarriers is  $N_c = 256$ , the number of transmit antennas is  $N_t = 64$ , the number of receive antennas is  $N_r = 64$ , and the number of pulses in a coherent processing interval is  $N_p = 1$ . Since it is sufficient to use only the range and DoA information to track the ToI, to reduce computational burdens, we do not conduct Doppler processing. Hence, it is safe to set  $N_p = 1$ . As a result, the pulse duration is  $T_p = M(T_c + T_o) = 6\mu\text{s}$ , the pulse repetition interval is  $T_r = T_p = 6\mu\text{s}$ , the coherent processing interval is  $T_i = N_p T_r = 6\mu\text{s}$ , the subcarrier spacing is  $\Delta_f = 1/T_o = 0.2\text{MHz}$ , the bandwidth is  $B = N_c \Delta_f = 51.2\text{MHz}$ , the sampling time interval and the range resolution is  $T_s = 1/B = 0.019531\mu\text{s}$ ,

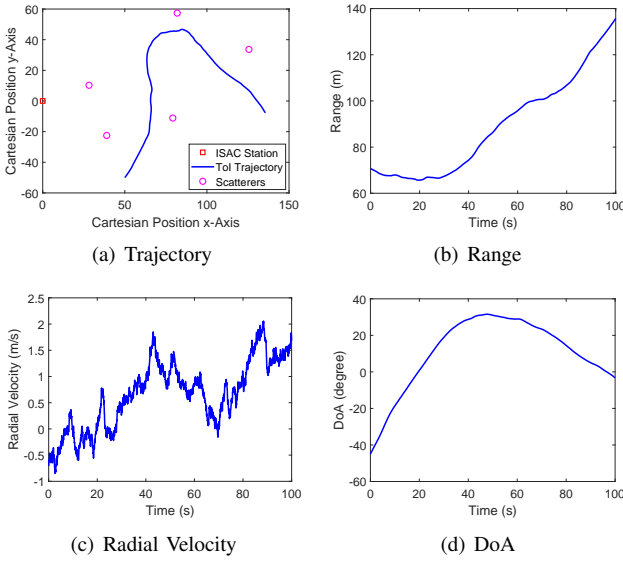


Fig. 2. Tracking the maneuvering ToI using CW MIMO-OFDM ISAC.

the resolution of sin-DoA (not DoA itself) is  $2/64 = 1/32$ . Let the SNR be  $-10\text{dB}$ , which is a practical and challenging case. In addition, we let the path gain of the ToI, at  $k$ , be

$$\beta_{k,0} = [0.9 + 0.1 \times (2r_{k,1} - 1)]e^{j2\pi r_{k,2}}, \quad (37)$$

where the random variable  $r_{k,1}$  is distributed according to the uniform distribution on  $[0, 1]$  and the random variable  $r_{k,2}$  is distributed according to the standard Gaussian distribution  $\mathcal{N}(0, 1)$ ; this formula is applicable for fast-fading channels. Hence, the ToI path gain is significantly time-varying across different tracking times  $k$ . The number of particles is set to  $N_{\text{par}} = 200$ , the effective particle number used in particle resampling is  $N_{\text{eff}} = N_{\text{par}}/2$ , and the power coefficient in (15) is  $\xi = 1$ . For other minor experimental settings, see the shared source codes at GitHub.

The tracking results for the 2-dimensional (2D) Cartesian positions are shown in Table I; the 2D position MSEs are averaged over all different  $k$ 's and independent Monte-Carlo (MC) trials, so are the running times (Time); however, we found that the empirical performance variations are not obvious across different MC episodes because MSEs are averaged on a long time trajectory indexed by  $k$ . From Table I, we can see that PF-SLTR is significantly better than PF-ILTR, PF-SLTR-A, and RBPF-SLTR-A, in terms of both computation and accuracy. This is because PF-ILTR must consume a huge amount of time to obtain the raw measurements of the ToI parameters  $(\tau_0, \nu_0, \theta_0)$ . Within a tracking time window of  $T_t = 50\text{ms}$ , spending  $814.1\text{ms}$  on computations is operationally intolerable because target tracking is a real-time signal processing problem. In contrast, the proposed PF-SLTR does not require this operation. In addition, the convergence of PF-SLTR-A and RBPF-SLTR-A is difficult to ensure for the following two reasons: First, it is challenging to accurately track the

quickly-jumping path gain  $\beta_{k,0}$  in (37);<sup>3</sup> second, the likelihood function in (35) and (36) is not sufficiently precise due to the presence of unknown scatterers. However, the proposed PF-SLTR in Algorithm 1 does not require estimating  $\beta_{k,0}$  or relying on the exact likelihood function, resulting in superior performance.

TABLE I  
TRACKING RESULTS FOR THE SCENARIO IN FIG. 2

	PF-SLTR	PF-ILTR	PF-SLTR-A	RBPF-SLTR-A
MSE	<b>0.0062</b>	2.4620	(Diverged)	(Diverged)
Time	<b>23.7</b>	814.1	30.2	30.0

Note: Unit for MSE:  $\text{m}^2$ ; unit for Time: ms.

In the following, we present the tracking results of PF-SLTR under different parameters. Results of other filters are not displayed because, as we can see, they are significantly dominated by PF-SLTR. When we vary one parameter, we keep the other the same as those used in Table I.

The tracking results for different numbers of particles are given in Table II. As expected, in particle filtering, due to the law of large numbers, the larger the number of particles, the less the average tracking error. However, as the number  $N_{\text{par}}$  of particles increases, more computing resources are required.

TABLE II  
TRACKING RESULTS OF PF-SLTR WHEN  $N_{\text{PAR}}$  VARIES

$N_{\text{par}}$	50	100	150	200
MSE (unit: $\text{m}^2$ )	0.0432	0.0129	0.0082	<b>0.0062</b>
Time (unit: ms)	6.2	12.4	18.3	<b>23.7</b>

Note: Boldfaced values are baselines in Table I.

The tracking results for different SNRs are given in Table III. As indicated, the proposed method is relatively insensitive to the value of SNR because a wide bandwidth (i.e., 256 subcarriers with the spacing of  $0.2\text{MHz}$ ) and a large antenna aperture (i.e., 64 receive and transmit antennas) are used in this experiment. However, the larger value of SNR indeed helps decrease the average tracking error, although moderately.

TABLE III  
TRACKING RESULTS OF PF-SLTR WHEN SNR VARIES

SNR	-20	<b>-10</b>	0	10
MSE (unit: $\text{m}^2$ )	0.0068	<b>0.0062</b>	0.0060	0.0057
Time (unit: ms)	23.4	<b>23.7</b>	23.7	24.1

Note: Boldfaced values are baselines in Table I.

The tracking results for different numbers of antennas are given in Table IV. As we can anticipate, the larger the number of antennas is, the smaller the average tracking error is, and the more the computational burden is.

The tracking results for different numbers of subcarriers are given in Table V. It suggests that, given subcarrier spacing,

<sup>3</sup>The random process  $\{\beta_{k,0}\}_k$  is independent and identically distributed over time  $k$ , and there is no correlation between  $\beta_{k-1,0}$  and  $\beta_{k,0}$ . However, in target tracking algorithms, such as the random walk and CV models, the first-order Markov property of  $\{\beta_{k,0}\}_k$  must be assumed as in (1), which, on the contrary, misleads the tracking filter.

TABLE IV  
TRACKING RESULTS OF PF-SLTR WHEN  $N_t$  AND  $N_r$  VARY

$N_t = N_r =$	8	16	32	<b>64</b>
MSE (unit: $m^2$ )	407.6502	0.0245	0.0085	<b>0.0062</b>
Time (unit: ms)	6.6	9.0	14.2	<b>23.7</b>

Note: Boldfaced values are baselines in Table I.

the more the number of subcarriers (i.e., the larger the bandwidth is), the smaller the average tracking error. However, this performance improvement comes with an increase in computational times.

TABLE V  
TRACKING RESULTS OF PF-SLTR WHEN  $N_c$  VARIES

$N_c$	32	64	128	<b>256</b>
MSE (unit: $m^2$ )	0.2975	0.0559	0.0197	<b>0.0062</b>
Time (unit: ms)	8.5	11.5	18.3	<b>23.7</b>

Note: Boldfaced values are baselines in Table I.

The tracking results for different values of  $\xi$  in (15) are given in Table VI. We do not report the running times because the value of  $\xi$  does not essentially affect the computational complexity. The results show that the value of  $\xi$ , which balances the relative importance of the  $y_k$ -data-evidence compared to the prior belief [cf. (11)], can potentially further improve the performance of PF-SLTR; see also Theorem 1. However, the empirically best value of  $\xi$  is problem-specific and tuned case by case. For the specific scenario in Fig. 2, we empirically found that the larger the value of  $\xi$ , the better the MSE performance; however, this may not be a general observation for other cases.

TABLE VI  
TRACKING RESULTS OF PF-SLTR WHEN  $\xi$  VARIES

$\xi$	0.50	0.75	<b>1</b>	1.25	1.50
MSE (unit: $m^2$ )	0.0091	0.0080	<b>0.0062</b>	0.0054	0.0047
$\xi$	1.75	2.00	2.25	2.50	2.75
MSE (unit: $m^2$ )	0.0041	0.0036	0.0034	0.0034	0.0031

Note: Boldfaced values are baselines in Table I.

## VI. CONCLUSIONS

This article proposes a new particle filtering framework to address core challenges in signal-level target tracking using MIMO multi-carrier pulse-Doppler radar. By adopting an optimization-centric interpretation of Bayes' rule, the proposed method eliminates the need for explicit likelihood models and avoids augmenting nuisance parameters (e.g., complex path gains) into the state vector. Instead, the filtering process is driven by evaluating the data evidence of each hypothesized target state using domain-tailored cost functions. This shift achieves significant performance improvements in both running times and tracking accuracy, relative to conventional approaches. Moreover, the proposed framework is adapted for implementation in MIMO-OFDM systems, enabling practical integration with existing communication infrastructures to realize joint sensing and communication capabilities. Both

the pulsed paradigm for tracking far and fast targets and the continuous-wave scheme for tracking near and slow targets are discussed. Simulation results confirm the effectiveness of the proposed approaches in diverse MIMO-OFDM ISAC configurations, demonstrating the real-time feasibility and reliable tracking performance under unknown likelihood models.

*Closing Notes:* To further extend the applicability of the proposed filtering framework to coordinated multi-point systems, a principled fusion strategy is introduced to aggregate particle-based posterior state distributions across distributed sensing stations. This strategy leverages the maximum entropy law and statistical optimality in the fusion of discrete distributions, which helps preserve particle diversity and mitigate particle degeneracy. For better readability and due to the page limit, see Appendix A.

## ACKNOWLEDGMENTS

The authors thank Prof. Simon J. Godsill of the University of Cambridge for his constructive comments on incorporating the Rao–Blackwellized particle filter into the discussions of this article.

## APPENDIX A COORDINATED MULTI-POINT SYSTEMS

### A. Motivations

To improve throughput and reliability in wireless communications, as well as accuracy and trustworthiness in wireless sensing, multi-point access is emerging as a potential solution [65], [66]. To enable the use of the proposed PF-SLTR in coordinated multi-point (i.e., multi-station, radar network) systems, an optimization-centric fusion strategy of posterior state distributions from multiple sensing stations is studied. The features of this fusion strategy are as follows:

- By using advanced statistical metrics of distributions, the new fusion strategy allows the fusion of a set of discrete distributions that have different supports, in contrast to the canonical fusion rule for common-support discrete distributions [67].
- By sampling particles from a larger region and maximizing the spread of the particle weights, compared to the single-station case, the new fusion strategy improves the diversity of the particles and the effectiveness of the associated weights, so that the impoverishment and degeneracy problems in particle filtering can be alleviated.

### B. Principles and Methods

This subsection studies the PF-SLTR for the multi-point ISAC systems, where each station first independently tracks the target and then all stations fuse the tracking results. This information fusion operation can significantly improve the accuracy of PF-SLTR.

Suppose that we have  $Z$  ISAC stations, indexed by  $z \in [Z]$ . Each station governs a posterior particle-represented ToI-parameter distribution

$$q_z(\mathbf{x}|\mathbf{y}) = \sum_{i=0}^{N_{\text{par}}-1} u_{z,i} \delta(\mathbf{x} - \mathbf{x}_{z,i}), \quad \forall z \in [Z]. \quad (38)$$

We aim to fuse these  $Z$  distributions to form an integrated  $N_{\text{par}}$ -atom discrete posterior distribution  $q(\mathbf{x}|\mathbf{y})$ :

$$q(\mathbf{x}|\mathbf{y}) = \sum_{i=0}^{N_{\text{par}}-1} u_i \delta(\mathbf{x} - \mathbf{x}_i) := \underset{z \in [Z]}{\text{fuse}} q_z(\mathbf{x}|\mathbf{y}), \quad (39)$$

where  $\{u_i\}_{i \in [N_{\text{par}}]}$  is the fused weights and  $\{\mathbf{x}_i\}_{i \in [N_{\text{par}}]}$  is the fused particles. Suppose that the minimum covering region of  $q(\mathbf{x}|\mathbf{y})$  and  $\{q_z(\mathbf{x}|\mathbf{y})\}_{z \in [Z]}$  is  $\mathcal{X}$ ; i.e., for every  $z \in [Z]$  and  $i \in [N_{\text{par}}]$ , we have  $\mathbf{x}_{z,i}, \mathbf{x}_i \in \mathcal{X}$ . For presentation clarity, hereafter in this subsection, the notational dependence of  $q(\mathbf{x}|\mathbf{y})$  and  $\{q_z(\mathbf{x}|\mathbf{y})\}_{z \in [Z]}$  on  $\mathbf{y}$  is omitted, because the fusion rule in this subsection applies to any collection of common-domain (i.e.,  $\mathcal{X}$ ) distributions, not limited to posterior distributions only.

To generate  $q(\mathbf{x})$ , we can randomly draw a set of particles  $\{\mathbf{x}_i\}_{i \in [N_{\text{par}}]}$  from  $\mathcal{X}$  (e.g., using stratified sampling of  $\{q_z(\mathbf{x})\}_{z \in [Z]}$ , uniform sampling on  $\mathcal{X}$ , etc.), and then determine their weights  $\{u_i\}_{i \in [N_{\text{par}}]}$ . In this importance-sampling procedure, however, the following two rules need to be taken into account:

- Particles  $\{\mathbf{x}_i\}_{i \in [N_{\text{par}}]}$  should be as diverse as possible on  $\mathcal{X}$ ; that is, particles should cover the whole space  $\mathcal{X}$  as much as they can. This rule is to combat the impoverishment issue in particle filtering.
- Weights  $\{u_i\}_{i \in [N_{\text{par}}]}$  should be as balanced as possible; that is, weights should have as few differences as they can. This rule aims to address the degeneracy issue in particle filtering.

The first rule of particle diversity can be easily satisfied in practice using the uniform sampling on  $\mathcal{X}$ . Nevertheless, the second rule of weight balancedness needs nontrivial treatment. A natural quantitative measure of balancedness on the probability simplex  $\{u_i\}_{i \in [N_{\text{par}}]}$  can be its entropy value; the larger the entropy value of a discrete distribution is, the more balanced this distribution is. In addition, considering that the  $Z + 1$  discrete distributions  $q(\mathbf{x})$  and  $\{q_z(\mathbf{x})\}_{z \in [Z]}$  have different support atoms, this article proposes the following optimization-centric fusion rule:

$$\begin{aligned} \min_{g(\mathbf{x})} \quad & - \int_{\mathcal{X}} -g(\mathbf{x}) \ln g(\mathbf{x}) d\mathbf{x} + \kappa \sum_{z=0}^{Z-1} \rho(g(\mathbf{x}), q_z(\mathbf{x})) \\ \text{s.t.} \quad & \int_{\mathcal{X}} g(\mathbf{x}) d\mathbf{x} = 1, \end{aligned} \quad (40)$$

which finds the maximum entropy (i.e., maximum spread) distribution that is simultaneously close to all  $\{q_z(\mathbf{x})\}_{z \in [Z]}$ ;  $\rho(g(\mathbf{x}), q_z(\mathbf{x}))$  defines the Wasserstein distance between  $g(\mathbf{x})$  and  $q_z(\mathbf{x})$  [68, Definition 6.1];  $\kappa \geq 0$  is a tradeoff parameter to compromise between the spread of  $g(\mathbf{x})$  and the overall closeness to all  $\{q_z(\mathbf{x})\}_{z \in [Z]}$ . Note that the larger the entropy value of a distribution, the more this distribution spreads over its domain, that is, the more diverse the realizations drawn from this distribution. Let  $g^*(\mathbf{x})$  solve Problem (40). The weights  $\{u_i\}_{i \in [N_{\text{par}}]}$  of the particles  $\{\mathbf{x}_i\}_{i \in [N_{\text{par}}]}$  can be determined by the principle of importance sampling, as follows

$$u_i \propto g^*(\mathbf{x}_i), \quad \forall i \in [N_{\text{par}}]. \quad (41)$$

The benefits of employing (40) and (41) are twofold:

- The distributions  $q(\mathbf{x})$  and  $\{q_z(\mathbf{x})\}_{z \in [Z]}$  on  $\mathcal{X}$  can have (significantly) different support atoms and weights;
- The weights  $\{u_i\}_{i \in [N_{\text{par}}]}$  can be as balanced as possible.

The last technical step is to efficiently solve Problem (40), whose solution is given in the theorem below.

*Theorem 2:* Suppose that the Wasserstein distance is of order 1 and induced by the norm  $\|\cdot\|$  on  $\mathcal{X}$ . The optimal distribution  $g^*(\mathbf{x})$  solving (40) is given by

$$g^*(\mathbf{x}) = \exp \left\{ -1 - v^* - \kappa \sum_{z=0}^{Z-1} \min_{i \in [N_{\text{par}}]} \left\{ \|\mathbf{x} - \mathbf{x}_{z,i}\| - \gamma_{z,i}^* \right\} \right\} \quad (42)$$

where  $v^*$  and  $\{\gamma_{z,i}^*\}_{z \in [Z], i \in [N_{\text{par}}]}$  solve the following unconstrained convex program

$$\begin{aligned} \max_{v, \{\gamma_{z,i}\}} \quad & \kappa \sum_{z=0}^{Z-1} \sum_{i=0}^{N_{\text{par}}-1} u_{z,i} \gamma_{z,i} - v - \\ & \int_{\mathcal{X}} \exp \left\{ -1 - v - \kappa \sum_{z=0}^{Z-1} \min_{i \in [N_{\text{par}}]} \left\{ \|\mathbf{x} - \mathbf{x}_{z,i}\| - \gamma_{z,i} \right\} \right\} d\mathbf{x}. \end{aligned} \quad (43)$$

*Proof:* See Appendix A-E.  $\square$

Because Problem (43) is convex and smooth in  $v$  and  $\gamma_{z,i}$ , for every  $z \in [Z]$  and  $i \in [N_{\text{par}}]$ , we can use gradient-based methods to solve it, e.g., gradient descent. The gradient with respect to  $v$  is

$$\begin{aligned} -1 + & \int_{\mathcal{X}} \exp \left\{ -1 - v - \kappa \sum_{z=0}^{Z-1} \min_{i \in [N_{\text{par}}]} \left\{ \|\mathbf{x} - \mathbf{x}_{z,i}\| - \gamma_{z,i} \right\} \right\} d\mathbf{x}, \end{aligned} \quad (44)$$

and that with respect to  $\gamma_{z,i}$ , for every  $z \in [Z], i \in [N_{\text{par}}]$ , is

$$\kappa \cdot \left\{ u_{z,i} - \int_{\mathcal{X}_{z,i}} \exp \left[ -1 - v - \kappa \left( \|\mathbf{x} - \mathbf{x}_{z,i}\| - \gamma_{z,i} \right) \right] d\mathbf{x} \right\}, \quad (45)$$

where  $\mathcal{X}_{z,i}$ , a subset of  $\mathcal{X}$ , is defined as

$$\begin{aligned} \mathcal{X}_{z,i} := & \left\{ \mathbf{x} \in \mathcal{X} : \|\mathbf{x} - \mathbf{x}_{z,i}\| - \gamma_{z,i} \leq \|\mathbf{x} - \mathbf{x}_{z,j}\| - \gamma_{z,j} \right\}, \\ & \forall j \in [N_{\text{par}}], j \neq i. \end{aligned} \quad (46)$$

Note that for every  $z \in [Z]$ , we have

$$\mathcal{X}_{z,i} \bigcap \mathcal{X}_{z,j} = \emptyset, \quad \text{if } i \neq j; \quad \text{and} \quad \mathcal{X} = \bigcup_{i=0}^{N_{\text{par}}-1} \mathcal{X}_{z,i}.$$

That is, for every  $z \in [Z]$ , the collection of sets  $\{\mathcal{X}_{z,i}\}_{i \in [N_{\text{par}}]}$  is a mutually exclusive and collectively exhaustive (MECE) partition of the whole space  $\mathcal{X}$ . The following points regarding the optimization (43), together with its gradients in (44) and (45), have to be outlined:

- Problem (43) is a large-scale unconstrained optimization in which  $1 + ZN_{\text{par}}$  real-valued variables are involved. However, the fusion formulation (40) is only designed for small  $N_{\text{par}}$  to combat particle impoverishment and

particle degeneracy. When  $N_{\text{par}}$  is relatively large, stratified sampling of  $\{q_z(\mathbf{x})\}_{\forall z \in [Z]}$  can be practically sufficient to achieve the same goal, because the particles  $\{\mathbf{x}_{z,i}\}_{\forall z \in [Z], i \in [N_{\text{par}}]}$  are diverse and well-spread on  $\mathcal{X}$ .

- When the gradients approach zeros, (44) implies that  $g^*(\mathbf{x})$  in (42) is indeed a probability distribution that has a unity integral, whereas (45) means that, for every  $z \in [Z]$ , the collection of sets  $\{\mathcal{X}_{z,i}\}_{\forall i \in [N_{\text{par}}]}$  is indeed an MECE partition of  $\mathcal{X}$ . Note that the integral of  $g^*(\mathbf{x})$  on the partition  $\mathcal{X}_{z,i}$  is  $u_{z,i}$ .
- In gradient evaluations, the integrals in (44) and (45) can be approximated using numerical methods, e.g., Monte-Carlo integration.

### C. Computational Complexity

If the multi-point coordination is adopted in a fusion center, at each tracking time  $k$ , the fusion center has the following three operations:

- 1) Uniformly sample  $N_{\text{par}}$  integrated particles from the minimum covering region  $\mathcal{X}$  (of particles from all stations);
- 2) Determine the weights of these particles using  $g^*(\mathbf{x})$  in (42), where the gradients are given in (44) and (45);
- 3) Distribute the fused particles and weights to stations, serving as their prior distributions in the next time step.

The computational complexity, in time, for this fusion process is  $\mathcal{O}(N_{\text{gd}}N_{\text{mci}}ZN_{\text{par}}d_x)$ , where  $N_{\text{gd}}$  is the running steps of gradient descent, and  $N_{\text{mci}}$  is the number of Monte-Carlo samples to numerically evaluate the integrals in (44) and (45). However, if  $N_{\text{par}}$  is relatively large, using stratified sampling of particle-represented  $\{q_z(\mathbf{x}_k|\mathbf{y}_k)\}_{\forall z \in [Z]}$  can be practically effective as a fusion rule to generate integrated particles with uniform weights; the compromise of this practical trick is that there is no explicit optimality guarantee as in (40).

### D. Experiments

In this subsection, we show the performance gain from the multi-point coordination in Table VII. The MSEs and running times are reported against the number  $Z$  of ISAC stations. Indeed, multi-point fusion can enhance tracking performance. However, this improvement comes at the cost of nontrivially increased computational complexity. Note that increasing the number of ISAC stations is not always beneficial, as the fusion gain in MSEs quickly saturates while the computational time grows substantially.

TABLE VII  
TRACKING RESULTS OF PF-SLTR WHEN  $Z$  VARIES

$Z$	1	2	3	4
MSE (unit: $\text{m}^2$ )	<b>0.0062</b>	0.0030	0.0022	0.0019
Time (unit: ms)	<b>23.7</b>	50.7	87.6	127.0

Note: Boldfaced values are baselines in Table I.

### E. Proof of Theorem 2

*Proof:* According to the finite-dimensional reformulation of Wasserstein distance between a continuous distribution  $q(\mathbf{x})$

and a discrete distribution  $q_z(\mathbf{x})$  [69, Lemma 1], the Lagrange dual problem of (40) can be written as (47).

Since the objective function is convex and constraint-free in terms of  $q(\mathbf{x})$ , and concave in terms of  $\{\gamma_{z,i}\}$ , the variational method can be used to maximize it over  $q(\mathbf{x})$ , leading to

$$\ln q(\mathbf{x}) + \kappa \sum_{z=0}^{Z-1} \min_{i \in N_{\text{par}}} \left\{ \|\mathbf{x} - \mathbf{x}_{z,i}\| - \gamma_{z,i} \right\} + v + 1 \equiv 0,$$

almost everywhere. This gives the form of  $q(\mathbf{x})$  in (42). Substituting  $q(\mathbf{x})$  back into the objective of the Lagrange dual problem gives (43).

The strong duality holds because the original problem (40) is convex. This completes the proof.  $\square$

## APPENDIX B PROOF OF PROPOSITION 1

*Proof:* Solve (19) with respect to  $\gamma$ , yielding

$$h_1(\mathbf{y}, \varphi) = \sum_{p=0}^{N_p-1} \sum_{l=0}^{L-1} \mathbf{y}_p^H(l) \mathbf{y}_p(l) - \frac{\left| \sum_{p=0}^{N_p-1} \sum_{l=0}^{L-1} \mathbf{y}_p^H(l) \mathbf{b}(\theta) \mathbf{a}^H(\theta) \mathbf{s}_p(l-\tau) e^{j2\pi p T_r \nu} \right|^2}{\sum_{p=0}^{N_p-1} \sum_{l=0}^{L-1} \mathbf{a}^H(\theta) \mathbf{s}_p(l-\tau) \mathbf{s}_p^H(l-\tau) \mathbf{a}(\theta) \mathbf{b}^H(\theta) \mathbf{b}(\theta)} \geq 0. \quad (48)$$

The denominator in the second line equals

$$N_r N_p \mathbf{a}^H(\theta) \sum_{l=0}^{L_{\text{ss}}-1} \mathbf{s}_p(l) \mathbf{s}_p^H(l) \mathbf{a}(\theta) = N_r N_p L_{\text{ss}} \mathbf{a}^H(\theta) \hat{\mathbf{R}}_s \mathbf{a}(\theta).$$

Note that  $L_{\text{ss}} \leq L$  and  $\mathbf{s}_p(l) = \mathbf{0}$  if  $L_{\text{ss}} \leq l \leq L-1$ , for every  $p \in [N_p]$ . This completes the proof.  $\square$

## APPENDIX C PROOF OF PROPOSITION 3

*Proof:* The frequency-domain signal model (5) can be written as

$$\bar{\mathbf{y}}_p(n) = \beta_0 \mathbf{b}(\theta_0) \mathbf{a}^H(\theta_0) \bar{\mathbf{s}}_p(n) e^{-j2\pi n \Delta \tau_0} e^{j2\pi n T_r \nu_0} + \bar{\mathbf{n}}_p(n),$$

where  $\bar{\mathbf{n}}_p(n)$  denotes the pure (i.e., scatterer-free) channel noise;  $\bar{\mathbf{n}}_p(n)$  is uncorrelated with  $\bar{\mathbf{s}}_p(n)$  for every  $n \in [N_{\text{cr}}]$  and  $p \in [N_p]$ . Hence, we have (49)-(51).

The first nulls of the Dirichlet function, or the periodic sinc function, in (51) is given by the following conditions in each independent dimension:  $\frac{N_t}{2}(\sin \theta_0 - \sin \theta) = \pm 1$ ,  $\frac{N_r}{2}(\sin \theta_0 - \sin \theta) = \pm 1$ ,  $B(\tau_0 - \tau) = \pm 1$ , and  $T_i(\nu - \nu_0) = \pm 1$ . Therefore, within the tracking gate

$$\left[ \tau_0 - \frac{1}{B}, \tau_0 + \frac{1}{B} \right] \times \left[ \nu_0 - \frac{1}{T_i}, \nu_0 + \frac{1}{T_i} \right] \times \left[ \arcsin \left( \sin \theta_0 - \frac{2}{N_{tr}} \right), \arcsin \left( \sin \theta_0 + \frac{2}{N_{tr}} \right) \right],$$

the Dirichlet function is nonzero and satisfies Rule 1. This completes the proof.  $\square$

$$\begin{aligned}
& \max_v \min_{q(\mathbf{x})} \int q(\mathbf{x}) \ln q(\mathbf{x}) d\mathbf{x} + \kappa \cdot \sum_{z=0}^{Z-1} \left\{ \max_{\{\gamma_{z,i}\}} \left[ \int q(\mathbf{x}) \min_{i \in [N_{\text{par}}]} \left\{ \|\mathbf{x} - \mathbf{x}_{z,i}\| - \gamma_{z,i} \right\} d\mathbf{x} \right] + \sum_{i=1}^{N_{\text{par}}} u_{z,i} \gamma_{z,i} \right\} + v \left[ \int q(\mathbf{x}) d\mathbf{x} - 1 \right] \\
&= \max_v \min_{q(\mathbf{x})} \max_{\{\gamma_{z,i}\}} \kappa \cdot \sum_{z=0}^{Z-1} \sum_{i=1}^{N_{\text{par}}} u_{z,i} \gamma_{z,i} - v + \int q(\mathbf{x}) \left[ \ln q(\mathbf{x}) + \kappa \cdot \sum_{z=0}^{Z-1} \left[ \min_{i \in [N_{\text{par}}]} \left\{ \|\mathbf{x} - \mathbf{x}_{z,i}\| - \gamma_{z,i} \right\} \right] + v \right] d\mathbf{x}.
\end{aligned} \tag{47}$$

$$\bar{\mathbf{y}}_p^H(n) \mathbf{b}(\theta) \mathbf{a}^H(\theta) \bar{\mathbf{s}}_p(n) e^{-j2\pi n \Delta \tau} e^{j2\pi p T_r \nu} = \beta_0^H \mathbf{b}^H(\theta) \mathbf{b}(\theta_0) \mathbf{a}^H(\theta_0) \bar{\mathbf{s}}_p(n) \bar{\mathbf{s}}_p^H(n) \mathbf{a}(\theta) e^{j2\pi n \Delta(\tau_0 - \tau)} e^{j2\pi p T_r(\nu - \nu_0)} + \bar{\mathbf{n}}_p^H(n) \mathbf{b}(\theta) \mathbf{a}^H(\theta) \bar{\mathbf{s}}_p(n) e^{-j2\pi n \Delta \tau} e^{j2\pi p T_r \nu} \tag{49}$$

$$\begin{aligned}
& \mathbb{E}_{\{\bar{\mathbf{y}}_p(n), \bar{\mathbf{s}}_p(n)\}_{\forall p,n}} \left\{ \sum_{p=0}^{N_p-1} \sum_{n=0}^{N_{\text{cr}}-1} \left[ \bar{\mathbf{y}}_p^H(n) \mathbf{b}(\theta) \mathbf{a}^H(\theta) \bar{\mathbf{s}}_p(n) e^{-j2\pi n \Delta \tau} e^{j2\pi p T_r \nu} \right] \right\} \\
&= \beta_0^H \mathbf{b}^H(\theta) \mathbf{b}(\theta_0) \mathbf{a}^H(\theta_0) \mathbf{R}_s \mathbf{a}(\theta) \sum_{n=0}^{N_{\text{cr}}-1} e^{j2\pi n \Delta(\tau_0 - \tau)} \sum_{p=0}^{N_p-1} e^{j2\pi p T_r(\nu - \nu_0)} + \\
&\quad \mathbb{E}_{\{\bar{\mathbf{n}}_p(n), \bar{\mathbf{s}}_p(n)\}_{\forall p,n}} \left\{ \mathbf{a}^H(\theta) \sum_{p=0}^{N_p-1} \sum_{n=0}^{N_{\text{cr}}-1} \bar{\mathbf{s}}_p(n) \bar{\mathbf{n}}_p^H(n) e^{-j2\pi n \Delta \tau} e^{j2\pi p T_r \nu} \mathbf{b}(\theta) \right\} \\
&= \beta_0^H P_t \mathbf{b}^H(\theta) \mathbf{b}(\theta_0) \mathbf{a}^H(\theta_0) \mathbf{a}(\theta) \sum_{n=0}^{N_{\text{cr}}-1} e^{j2\pi n \Delta(\tau_0 - \tau)} \sum_{p=0}^{N_p-1} e^{j2\pi p T_r(\nu - \nu_0)} + 0 \\
&= \beta_0^H P_t \sum_{t=0}^{N_t-1} e^{j\pi t(\sin \theta - \sin \theta_0)} \sum_{r=0}^{N_r-1} e^{j\pi r(\sin \theta_0 - \sin \theta)} \sum_{n=0}^{N_{\text{cr}}-1} e^{j2\pi n \Delta(\tau_0 - \tau)} \sum_{p=0}^{N_p-1} e^{j2\pi p T_r(\nu - \nu_0)} \\
&= \beta_0^H P_t \sum_{t=0}^{N_t-1} e^{j2\pi \frac{t}{N_t} \frac{N_t}{2} (\sin \theta - \sin \theta_0)} \sum_{r=0}^{N_r-1} e^{j2\pi \frac{r}{N_r} \frac{N_r}{2} (\sin \theta_0 - \sin \theta)} \sum_{n=0}^{N_{\text{cr}}-1} e^{j2\pi \frac{n}{N_{\text{cr}}} B(\tau_0 - \tau)} \sum_{p=0}^{N_p-1} e^{j2\pi \frac{p}{N_p} T_i(\nu - \nu_0)}
\end{aligned} \tag{50}$$

$$|(50)| = |\beta_0| \cdot P_t \cdot \left| \frac{\sin[\pi \cdot (\frac{N_t}{2}(\sin \theta - \sin \theta_0))]}{\sin[\pi \cdot (\frac{N_t}{2}(\sin \theta - \sin \theta_0))/N_t]} \right| \cdot \left| \frac{\sin[\pi \cdot (\frac{N_r}{2}(\sin \theta_0 - \sin \theta))]}{\sin[\pi \cdot (\frac{N_r}{2}(\sin \theta_0 - \sin \theta))/N_r]} \right| \cdot \left| \frac{\sin[\pi \cdot (B(\tau_0 - \tau))]}{\sin[\pi \cdot (B(\tau_0 - \tau))/N_{\text{cr}}]} \right| \cdot \left| \frac{\sin[\pi \cdot (T_i(\nu - \nu_0))]}{\sin[\pi \cdot (T_i(\nu - \nu_0))/N_p]} \right| \tag{51}$$

## APPENDIX D PROOF OF THEOREM 1

*Proof:* We have

$$\begin{aligned}
\left[ - \sum_{i=0}^{N_{\text{par}}-1} \alpha_i^{(\xi)} \ln \alpha_i^{(\xi)} \right] &= \sum_{i=0}^{N_{\text{par}}-1} -\frac{\alpha_i^{(\xi)}}{C_\xi} \ln \frac{\alpha_i^{(\xi)}}{C_\xi} \\
&= \sum_{i=0}^{N_{\text{par}}-1} -\frac{\alpha_i^{(\xi)}}{C_\xi} \ln \alpha_i^{(\xi)} + \frac{\alpha_i^{(\xi)}}{C_\xi} \ln C_\xi \\
&= \frac{C_\xi \ln C_\xi}{C_\xi} - \frac{\xi}{C_\xi} \sum_{i=0}^{N_{\text{par}}-1} \alpha_i^{(\xi)} \ln \alpha_i.
\end{aligned}$$

The derivative with respect to  $\xi$  is

$$\frac{\xi}{C_\xi^2} \left\{ \left[ \sum_{i=0}^{N_{\text{par}}-1} \alpha_i^{(\xi)} \ln \alpha_i \right]^2 - \left[ \sum_{i=0}^{N_{\text{par}}-1} \alpha_i^{(\xi)} \right] \left[ \sum_{i=0}^{N_{\text{par}}-1} \alpha_i^{(\xi)} \ln \alpha_i \ln \alpha_i \right] \right\} \leq 0,$$

where the inequality is due to the Cauchy inequality, and the equality holds if and only if  $\alpha$  is a uniform distribution.

Therefore, the entropy function  $\xi \mapsto - \sum_{i=0}^{N_{\text{par}}-1} \alpha_i^{(\xi)} \ln \alpha_i^{(\xi)}$  is monotonically decreasing in  $\xi \geq 0$ .  $\square$

## REFERENCES

- [1] K. V. Mishra, M. B. Shankar, V. Koivunen, B. Ottersten, and S. A. Vorobyov, "Toward millimeter-wave joint radar communications: A signal processing perspective," *IEEE Signal Processing Mag.*, vol. 36, no. 5, pp. 100–114, 2019.
- [2] F. Liu, L. Zheng, Y. Cui, C. Masouros, A. P. Petropulu, H. Griffiths, and Y. C. Eldar, "Seventy years of radar and communications: The road from separation to integration," *IEEE Signal Processing Mag.*, vol. 40, no. 5, pp. 106–121, 2023.
- [3] F. Liu, W. Yuan, C. Masouros, and J. Yuan, "Radar-assisted predictive beamforming for vehicular links: Communication served by sensing," *IEEE Trans. Wireless Commun.*, vol. 19, no. 11, pp. 7704–7719, 2020.
- [4] F. Dong, F. Liu, S. Lu, Y. Xiong, Q. Zhang, Z. Feng, and F. Gao, "Communication-assisted sensing in 6G networks," *IEEE J. Sel. Areas in Commun.*, vol. 43, pp. 1371–1386, 2025.
- [5] M. A. Richards, *Fundamentals of Radar Signal Processing*, 3rd ed. McGraw-Hill New York, 2022.
- [6] Z. Zhang, L. Chen, J. Xing, K. Liu, and Q. Chang, "Sensing-assisted intelligent transportation system with adaptive power allocation and automatic beam control," *IEEE Trans. Intell. Transp. Syst.*, vol. 26, pp. 8820–8833, 2025.
- [7] L. Lu, G. Y. Li, A. L. Swindlehurst, A. Ashikhmin, and R. Zhang, "An overview of massive MIMO: Benefits and challenges," *IEEE J. Sel. Topics Signal Processing*, vol. 8, no. 5, pp. 742–758, 2014.

[8] Y. Li, N. Seshadri, and S. Ariyavisitakul, "Channel estimation for OFDM systems with transmitter diversity in mobile wireless channels," *IEEE J. Sel. Areas in Commun.*, vol. 17, no. 3, pp. 461–471, 1999.

[9] Y. G. Li, J. H. Winters, and N. R. Sollenberger, "MIMO-OFDM for wireless communications: Signal detection with enhanced channel estimation," *IEEE Trans. Commun.*, vol. 50, no. 9, pp. 1471–1477, 2002.

[10] P. Stoica, J. Li, and Y. Xie, "On probing signal design for MIMO radar," *IEEE Trans. Signal Processing*, vol. 55, no. 8, pp. 4151–4161, 2007.

[11] L. Xu, J. Li, and P. Stoica, "Target detection and parameter estimation for MIMO radar systems," *IEEE Trans. Aerosp. Electron. Syst.*, vol. 44, no. 3, pp. 927–939, 2008.

[12] G. Cui, H. Li, and M. Rangaswamy, "MIMO radar waveform design with constant modulus and similarity constraints," *IEEE Trans. Signal Processing*, vol. 62, no. 2, pp. 343–353, 2013.

[13] V. Koivunen, M. F. Keskin, H. Wymeersch, M. Valkama, and N. González-Prelicic, "Multicarrier ISAC: Advances in waveform design, signal processing, and learning under nonidealities," *IEEE Signal Processing Mag.*, vol. 41, no. 5, pp. 17–30, 2024.

[14] Y. Zhang, S. Aditya, and B. Clerckx, "Input distribution optimization in OFDM dual-function radar-communication systems," *IEEE Trans. Signal Processing*, vol. 72, pp. 5258–5273, 2024.

[15] C. Sturm and W. Wiesbeck, "Waveform design and signal processing aspects for fusion of wireless communications and radar sensing," *Proc. IEEE*, vol. 99, no. 7, pp. 1236–1259, 2011.

[16] Z. Xiao, R. Liu, M. Li, Q. Liu, and A. L. Swindlehurst, "A novel joint angle-range-velocity estimation method for MIMO-OFDM ISAC systems," *IEEE Trans. Signal Processing*, vol. 72, pp. 3805–3818, 2024.

[17] M. F. Keskin, H. Wymeersch, and V. Koivunen, "Monostatic sensing with OFDM under phase noise: From mitigation to exploitation," *IEEE Trans. Signal Processing*, vol. 71, pp. 1363–1378, 2023.

[18] S. Mercier, S. Bidon, D. Roque, and C. Enderli, "Comparison of correlation-based OFDM radar receivers," *IEEE Trans. Aerosp. Electron. Syst.*, vol. 56, no. 6, pp. 4796–4813, 2020.

[19] G. San Antonio, D. R. Fuhrmann, and F. C. Robey, "MIMO radar ambiguity functions," *IEEE J. Sel. Topics Signal Processing*, vol. 1, no. 1, pp. 167–177, 2007.

[20] Y. Xiong, F. Liu, Y. Cui, W. Yuan, T. X. Han, and G. Caire, "On the fundamental tradeoff of integrated sensing and communications under Gaussian channels," *IEEE Trans. Inform. Theory*, vol. 69, no. 9, pp. 5723–5751, 2023.

[21] N. R. Olson, J. G. Andrews, and R. W. Heath, "Coverage and rate of joint communication and parameter estimation in wireless networks," *IEEE Trans. Inform. Theory*, vol. 70, no. 1, pp. 206–243, 2023.

[22] M. Ahmadipour, M. Kobayashi, M. Wigger, and G. Caire, "An information-theoretic approach to joint sensing and communication," *IEEE Trans. Inform. Theory*, vol. 70, no. 2, pp. 1124–1146, 2022.

[23] F. Liu, Y. Zhang, Y. Xiong, S. Li, W. Yuan, F. Gao, S. Jin, and G. Caire, "CP-OFDM achieves the lowest average ranging sidelobe under QAM/PSK constellations," *IEEE Trans. Inform. Theory*, vol. 71, pp. 6950–6967, 2025.

[24] C. R. Berger, B. Demissie, J. Heckenbach, P. Willett, and S. Zhou, "Signal processing for passive radar using OFDM waveforms," *IEEE J. Sel. Topics Signal Processing*, vol. 4, no. 1, pp. 226–238, 2010.

[25] L. Zheng and X. Wang, "Super-resolution delay-Doppler estimation for OFDM passive radar," *IEEE Trans. Signal Processing*, vol. 65, no. 9, pp. 2197–2210, 2017.

[26] M. Wu and C. Hao, "Super-resolution TOA and AOA estimation for OFDM radar systems based on compressed sensing," *IEEE Trans. Aerosp. Electron. Syst.*, vol. 58, no. 6, pp. 5730–5740, 2022.

[27] X. Hu, C. Masouros, F. Liu, and R. Nissel, "Low-PAPR DFRC MIMO-OFDM waveform design for integrated sensing and communications," in *ICC 2022-IEEE International Conference on Communications*. IEEE, 2022, pp. 1599–1604.

[28] P. Li, M. Li, R. Liu, Q. Liu, and A. L. Swindlehurst, "MIMO-OFDM ISAC waveform design for range-Doppler sidelobe suppression," *IEEE Trans. Wireless Commun.*, vol. 24, pp. 1001–1015, 2025.

[29] F. Liu, Y.-F. Liu, A. Li, C. Masouros, and Y. C. Eldar, "Cramér-Rao bound optimization for joint radar-communication beamforming," *IEEE Trans. Signal Processing*, vol. 70, pp. 240–253, 2021.

[30] S. Lu, F. Liu, F. Dong, Y. Xiong, J. Xu, Y.-F. Liu, and S. Jin, "Random ISAC signals deserve dedicated precoding," *IEEE Trans. Signal Processing*, vol. 72, pp. 3453–3469, 2024.

[31] Z. Du, F. Liu, Y. Xiong, T. X. Han, Y. C. Eldar, and S. Jin, "Reshaping the ISAC tradeoff under OFDM signaling: A probabilistic constellation shaping approach," *IEEE Trans. Signal Processing*, vol. 72, pp. 4782–4797, 2024.

[32] F. Liu, Y. Xiong, S. Lu, S. Li, W. Yuan, C. Masouros, S. Jin, and G. Caire, "Uncovering the iceberg in the sea: Fundamentals of pulse shaping and modulation design for random ISAC signals," *IEEE Trans. Signal Processing*, vol. 73, pp. 2511–2526, 2025.

[33] T. Xu, F. Liu, C. Masouros, and I. Darwazeh, "An experimental proof of concept for integrated sensing and communications waveform design," *IEEE Open J. Commun. Soc.*, vol. 3, pp. 1643–1655, 2022.

[34] F. Gu, P. Zhu, Y. Jiang, D. Wang, and Y. Wang, "Beam tracking for distributed millimeter-wave MIMO-OFDM systems with unscented particle filter," in *2023 IEEE 23rd International Conference on Communication Technology (ICCT)*. IEEE, 2023, pp. 534–539.

[35] X. R. Li and V. P. Jilkov, "Survey of maneuvering target tracking: Part I. dynamic models," *IEEE Trans. Aerosp. Electron. Syst.*, vol. 39, no. 4, pp. 1333–1364, 2003.

[36] S. Herbert, J. R. Hopgood, and B. Mulgrew, "MMSE adaptive waveform design for active sensing with applications to MIMO radar," *IEEE Trans. Signal Processing*, vol. 66, no. 5, pp. 1361–1373, 2017.

[37] M. S. Arulampalam, S. Maskell, N. Gordon, and T. Clapp, "A tutorial on particle filters for online nonlinear/non-Gaussian Bayesian tracking," *IEEE Trans. Signal Processing*, vol. 50, no. 2, pp. 174–188, 2002.

[38] D. Simon, *Optimal State Estimation: Kalman, H-Infinity, and Nonlinear Approaches*. John Wiley & Sons, 2006.

[39] S. Godsill, "Particle filtering: the first 25 years and beyond," in *ICASSP 2019-2019 IEEE International Conference on Acoustics, Speech and Signal Processing (ICASSP)*. IEEE, 2019, pp. 7760–7764.

[40] P. Ratnupairoj, W. Kongprawechnon, K. Fukawa, and K. Kaemarungsi, "A particle filter for objects tracking in cognitive MIMO system," in *2015 6th International Conference of Information and Communication Technology for Embedded Systems (IC-ICTES)*. IEEE, 2015, pp. 1–4.

[41] W. Huleihel, J. Tabrikian, and R. Shavit, "Optimal adaptive waveform design for cognitive MIMO radar," *IEEE Trans. Signal Processing*, vol. 61, no. 20, pp. 5075–5089, 2013.

[42] S. Wang, "Distributionally robust state estimation for jump linear systems," *IEEE Trans. Signal Processing*, vol. 71, pp. 3835–3851, 2023.

[43] X. R. Li and V. P. Jilkov, "Survey of maneuvering target tracking: Part III. measurement models," in *Signal and Data Processing of Small Targets 2001*, vol. 4473. SPIE, 2001, pp. 423–446.

[44] L. D. Stone, R. L. Streit, T. L. Corwin, and K. L. Bell, *Bayesian Multiple Target Tracking*, 2nd ed. Artech House, 2014.

[45] S. J. Davey, "SNR limits on Kalman filter detect-then-track," *IEEE Signal Processing Lett.*, vol. 20, no. 8, pp. 767–770, 2013.

[46] S. Herbert, J. R. Hopgood, and B. Mulgrew, "Computationally simple MMSE (A-optimal) adaptive beam-pattern design for MIMO active sensing systems via a linear-Gaussian approximation," *IEEE Trans. Signal Processing*, vol. 66, no. 18, pp. 4935–4945, 2018.

[47] S. J. Davey, M. G. Rutten, and B. Cheung, "A comparison of detection performance for several track-before-detect algorithms," *EURASIP Journal on Advances in Signal Processing*, vol. 2008, pp. 1–10, 2007.

[48] S. J. Davey, M. G. Rutten, and N. J. Gordon, "Track-before-detect techniques," *Integrated Tracking, Classification, and Sensor Management*, pp. 311–362, 2013.

[49] J. A. Zhang, F. Liu, C. Masouros, R. W. Heath, Z. Feng, L. Zheng, and A. Petropulu, "An overview of signal processing techniques for joint communication and radar sensing," *IEEE J. Sel. Topics Signal Processing*, vol. 15, no. 6, pp. 1295–1315, 2021.

[50] A. Doucet, N. De Freitas, N. J. Gordon *et al.*, *Sequential Monte Carlo methods in Practice*. Springer, 2001, vol. 1, no. 2.

[51] C. Snyder, T. Bengtsson, P. Bickel, and J. Anderson, "Obstacles to high-dimensional particle filtering," *Monthly Weather Review*, vol. 136, no. 12, pp. 4629–4640, 2008.

[52] T. Schon, F. Gustafsson, and P.-J. Nordlund, "Marginalized particle filters for mixed linear/nonlinear state-space models," *IEEE Trans. Signal Processing*, vol. 53, no. 7, pp. 2279–2289, 2005.

[53] O. Cappé, S. J. Godsill, and E. Moulines, "An overview of existing methods and recent advances in sequential Monte Carlo," *Proc. IEEE*, vol. 95, no. 5, pp. 899–924, 2007.

[54] P. Germain, F. Bach, A. Lacoste, and S. Lacoste-Julien, "PAC-Bayesian theory meets Bayesian inference," *Advances in Neural Information Processing Systems*, vol. 29, 2016.

[55] P. G. Bissiri, C. C. Holmes, and S. G. Walker, "A general framework for updating belief distributions," *Journal of the Royal Statistical Society Series B: Statistical Methodology*, vol. 78, no. 5, pp. 1103–1130, 2016.

[56] J. Knoblauch, J. Jlewson, and T. Damoulas, "An optimization-centric view on Bayes' rule: Reviewing and generalizing variational inference," *Journal of Machine Learning Research*, vol. 23, no. 132, pp. 1–109, 2022.

- [57] Y. Baek, W. Aquino, and S. Mukherjee, "Generalized Bayes approach to inverse problems with model misspecification," *Inverse Problems*, vol. 39, no. 10, p. 105011, 2023.
- [58] R. Martin and N. Syring, "Direct Gibbs posterior inference on risk minimizers: Construction, concentration, and calibration," in *Handbook of Statistics*. Elsevier, 2022, vol. 47, pp. 1–41.
- [59] G. Lellouch, A. Mishra, and M. Inggs, "Processing alternatives in OFDM radar," in *2014 International Radar Conference*. IEEE, 2014, pp. 1–6.
- [60] J. Kwon, N. Kwak, E. Yang, and K. Kim, "Particle filter based track-before-detect method in the range-Doppler domain," in *2019 IEEE Radar Conference (RadarConf)*. IEEE, 2019, pp. 1–5.
- [61] J. Vermaak, S. J. Godsill, and P. Perez, "Monte Carlo filtering for multi target tracking and data association," *IEEE Trans. Aerosp. Electron. Syst.*, vol. 41, no. 1, pp. 309–332, 2005.
- [62] N. Ito and S. Godsill, "A multi-target track-before-detect particle filter using superpositional data in non-Gaussian noise," *IEEE Signal Processing Lett.*, vol. 27, pp. 1075–1079, 2020.
- [63] R. W. Heath, N. Gonzalez-Prelcic, S. Rangan, W. Roh, and A. M. Sayeed, "An overview of signal processing techniques for millimeter wave MIMO systems," *IEEE J. Sel. Topics Signal Processing*, vol. 10, no. 3, pp. 436–453, 2016.
- [64] M. S. Davis, *MIMO Radar*. SciTech Publishing, Edison, NJ, 2013, ch. Chapter 4, pp. 119–145.
- [65] G. Li, S. Wang, K. Ye, M. Wen, D. W. K. Ng, and M. Di Renzo, "Multi-point integrated sensing and communication: Fusion model and functionality selection," *IEEE Wireless Commun. Lett.*, vol. 11, no. 12, pp. 2660–2664, 2022.
- [66] K. Meng, C. Masouros, A. P. Petropulu, and L. Hanzo, "Cooperative ISAC networks: Opportunities and challenges," *IEEE Wireless Commun.*, vol. 32, pp. 212–219, 2025.
- [67] G. Koliander, Y. El-Laham, P. M. Djurić, and F. Hlawatsch, "Fusion of probability density functions," *Proc. IEEE*, vol. 110, no. 4, pp. 404–453, 2022.
- [68] C. Villani, *Optimal Transport: Old and New*. Springer, 2009.
- [69] S. Wang, "Distributionally robust state estimation for nonlinear systems," *IEEE Trans. Signal Processing*, vol. 70, pp. 4408–4423, 2022.